ABSTRACT OF THESIS

Name of Candidate Andrew James MATHESON

Address

Degree Doctor of Philosophy *Date* May, 1962

Title of Thesis "MEASUREMENTS OF THE RELAXATION TIMES OF TETRAHEDRAL MOLECULES"

The translational-vibrational relaxation times of methane, tetradeuteromethane, silane and tetradeuterosilane have been measured by the ultrasonic method at 298° and 348° K. The usual theories of intermolecular energy transfer in gases predict that the deuterated molecules should have shorter relaxation times than the unsubstituted molecules. Experimentally it is found that the deuterated molecules have the longer relaxation times. The explanation offered is that, in these molecules and in other molecules with low moments of inertia, vibrational-rotational energy transfer takes place more rapidly than vibrational-translational energy transfer. The two lines on the Lambert-Salter correlation plot for relaxation times thus probably represent two different mechanisms of energy transfer. The effect of various catalysts in promoting vibrational de-excitation is also discussed, and it is shown that their relative efficiencies are consistent with the hypothesis of vibrational-rotational energy transfer. An approximate calculation is made to predict the relaxation times of the methanes and the silanes if vibrational-rotational energy transfer is taking place. This shows that the calculated effect of isotopic substitution agrees with the experimental results.

Use other side if necessary.

MEASUREMENTS OF THE RELAXATION TIMES OF TETRAHEDRAL MOLECULES

By

ANDREW J. MATHESON

Thesis presented for the degree of
Doctor of Philosophy.

University of Edinburgh.

May, 1962.

CONTENTS

SUMMARY

The translational-vibrational relaxation times of methane, tetradeuteromethane, silane and tetradeuterosilane have been measured by the ultrasonic method at 298° and 348°K. The usual theories of intermolecular energy transfer in gases predict that the deuterated molecules should have shorter relaxation times than the unsubstituted molecules. Experimentally it is found that the deuterated molecules have the longer relaxation times. The explanation offered is that, in these molecules and in other molecules with low moments of inertia, vibrational-rotational energy transfer takes place more rapidly than vibrational-translational energy transfer. The two lines on the Lambert-Salter correlation plot for relaxation times thus probably represent two different mechanisms of energy transfer. The effect of various catalysts in promoting vibrational de-excitation is also discussed, and it is shown that their relative efficiencies are consistent with the hypothesis of vibrational-rotational energy transfer. An approximate calculation is made to predict the relaxation times of the methanes and the silanes if vibrational-rotational energy transfer is taking place. This shows that the calculated effect of isotopic substitution agrees with the experimental results.

CHAPTER 1

INTRODUCTION

Energy in gases is distributed throughout the translational, vibrational and rotational modes. These degrees of freedom are in thermal equilibrium with one another, and intermolecular energy transfer among the various modes takes place by collisions of the gas molecules. The transfer of energy between rotation and translation is a relatively easy process and occurs at almost every collision. Vibrational energy transfer occurs less readily, however, and the time taken for energy to be transferred to, or "relax" from the translational to the vibrational mode of a molecule is known as the translational-vibrational relaxation time.

In order to measure translational-vibrational relaxation times some means must be found of imparting energy selectively to either the translational or the vibrational mode, and of measuring the time taken for energy to be transferred to the other mode. A convenient method of doing this is by measuring the velocity of high-frequency sound waves, In an ideal gas the velocity of sound, V, is given by:

$$V^2 = \gamma RT/M = \left(1 + \frac{R}{C_v}\right) \frac{RT}{M} \quad \ldots\ldots\ldots\ldots (1)$$

where C_v is the molar heat capacity at constant volume, γ is the ratio of the specific heats, R is the gas constant, T is the absolute temperature, and M is the molecular weight. Now C_v is the sum of the contributions to the specific heat of the translational, vibrational and rotational modes, giving

$$V^2 = \left[1 + \frac{R}{C_{trans} + C_{vib} + C_{rot}} \right] \frac{RT}{M} \quad \ldots\ldots\ldots (2)$$

At low sound frequencies the time interval between successive compressions and rarefactions of the gas is comparatively long, and there is plenty of time for excess translational energy to relax into the vibrational mode. The velocity of sound is thus independent of frequency at low frequencies. But as the sound frequency increases, the period of the sound wave becomes of the same order as the relaxation time. A rarefaction in the sound wave then succeeds a compression so quickly that the excess translational energy of a molecule is removed before it has time to transfer to vibration. The vibrational modes are now no longer able to contribute to the specific heat, that is $C_{vib} = 0$, and this decrease in the effective specific heat leads to an increase in the velocity of sound - Fig. 1.

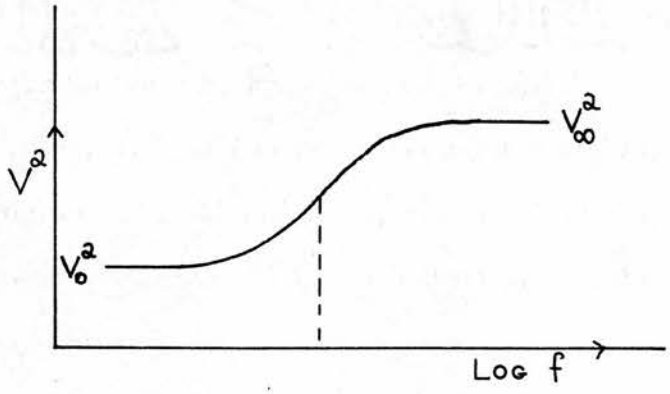

FIG. 1 — DISPERSION CURVE

The mid point of this dispersion curve corresponds to a sound wave whose period is proportional to the relaxation time.

The object of this work is to measure the relaxation times of the four tetrahedral molecules - methane, tetradeuteromethane, silane and

tetradeuterosilane. They provide a series of closely related molecules whose structure and properties are well known, and the deuterated molecules differ only in molecular weight and vibration frequencies. The effect of replacing hydrogen by deuterium had previously been investigated for only one compound. The results obtained have been interpreted in terms of a new mechanism of energy transfer in these molecules.

CHAPTER 2

SOUND PROPAGATION IN GASES

1. Velocity of sound in an ideal gas

It can be simply shown that sound waves of any shape are transmitted through a medium of density ρ and pressure p with phase velocity V given by

$$V^2 = \frac{dp}{d\rho} \qquad \ldots\ldots\ldots\ldots (3)$$

The processes in a sound wave are adiabatic, reversible and isentropic, and for an ideal gas this is expressed by pV^{γ} = constant, or

$$p = k\rho^{\gamma} \qquad \ldots\ldots\ldots\ldots (4)$$

Differentiating (4), and using pv = RT for 1 mole, gives

$$V^2 = \gamma\frac{p}{\rho} = \gamma\frac{RT}{M} = \frac{RT}{M}\left(1 + \frac{R}{C_v}\right) \ldots\ldots\ldots (1)$$

2. Correction of the observed velocity of sound to the ideal gas state.

Depending on the nature of the gas, the observed velocity of sound in a real gas may be greater or less than the velocity would be in the ideal gas. Since $\rho v = M$, equation (3) may be rewritten

$$V^2 = -\frac{v^2}{M}\left(\frac{\partial p}{\partial v}\right)_S \qquad \ldots\ldots\ldots\ldots (5)$$

Now $\left(\frac{\partial p}{\partial v}\right)_S = \gamma\left(\frac{\partial p}{\partial v}\right)_T$, by Reech's theorem

$$\therefore V^2 = -\gamma\frac{v^2}{M}\left(\frac{\partial p}{\partial v}\right)_T \qquad \ldots\ldots\ldots\ldots (6)$$

At moderate pressures the equation of state for a real gas may be expressed

$$pv = RT + Bp \qquad \ldots\ldots\ldots\ldots (7)$$

where B is the second virial coefficient. Combining this with (6) and neglecting powers of B higher than the first gives the velocity of sound in a real gas:

$$V^2 = \frac{\gamma}{M}(RT + 2Bp) \quad \ldots\ldots\ldots (8)$$

Roberts[1] derives the following relations, the subscripts referring to the ideal gas state:

$$C_p = C_{p_o} - Tp\frac{d^2B}{dT^2} \quad \ldots\ldots\ldots (9)$$

$$\text{and} \quad C_v = C_{v_o} - p\left(2\frac{dB}{dT} + T\cdot\frac{d^2B}{dT^2}\right) \ldots (10)$$

Dividing (9) by (10) and neglecting all products of differentials gives

$$\gamma = \gamma_o\left[1 + \frac{2p}{C_{v_o}}\cdot\frac{dB}{dT} + \frac{pRT}{C_{p_o}.C_{v_o}}\cdot\frac{d^2B}{dT^2}\right] \ldots. (11)$$

Substitute this value of γ in (8) and neglect all products of B with differentials,

$$V^2 = \frac{\gamma_o RT}{M}\left[1 + \frac{2p}{RT}\left(B + \frac{RT}{C_{v_o}}\cdot\frac{dB}{dT} + \frac{R^2T^2}{2C_{v_o}(C_{v_o}+R)}\frac{d^2B}{dT^2}\right)\right]$$

$$= V_o^2\left[1 + \frac{2Sp}{RT}\right]$$

$$\text{Thus} \quad V = V_o\left[1 + \frac{Sp}{RT}\right] \quad \ldots\ldots\ldots\ldots (12)$$

$$\text{where } S = B + \frac{T}{c}\cdot\frac{dB}{dT} + \frac{T^2}{2c(c+1)}\cdot\frac{d^2B}{dT^2} \quad \text{and} \quad c = \frac{C_{v_o}}{R}.$$

3. Derivation of the equations for relaxation.

Consider a gas with only one vibrational mode of frequency ν which becomes inoperative as the sound frequency increases. The energy

difference between the ground vibrational level and the first excited state, $E = h\nu$, is assumed to be such that only the first excited state is appreciably populated. Let N be the total number of molecules, N_0 be the number in the ground state, and N_1 the number in the first excited state. Then $N_0 + N_1 = N$, and at equilibrium $\overline{N_1} = \overline{N_0} \exp(-\frac{h\nu}{kT})$. Let f_{01}, f_{10} be the transition probabilities per molecule per second for the $0 \rightarrow 1$ and the $1 \rightarrow 0$ transitions. The rate of formation of excited molecules is

$$\frac{dN_1}{dt} = f_{01}N_0 - f_{10}N_1 \quad \ldots\ldots\ldots\ldots (13)$$

At equilibrium when $\frac{dN_1}{dt} = \frac{dN_0}{dt} = 0$,

$$\frac{f_{01}}{f_{10}} = \frac{\overline{N_1}}{\overline{N_0}} = \exp\left(-\frac{h\nu}{kT}\right) \ldots\ldots (14)$$

Let the system now be perturbed from equilibrium by a small amount so that N_1 is increased to $N_1 + \Delta N_1$. Within the limits of irreversible thermodynamics, we may say

$$\frac{d(\Delta N_1)}{dt} = -\frac{\Delta N_1}{\tau} \quad \ldots\ldots\ldots (15)$$

where τ is the time which elapses until the departure from equilibrium is reduced to $\frac{1}{e}$ of its original value. Also, from equation (13),

$$\frac{d(\overline{N_1} + \Delta N_1)}{dt} = f_{01}(\overline{N_0} - \Delta N_1) - f_{10}(\overline{N_1} + \Delta N_1)$$

Combining this with equations (15) and (14) we obtain

$$\frac{1}{\tau} = f_{10} + f_{01} \quad \ldots\ldots\ldots (16),$$

an expression for the relaxation time in terms of the transition probabilities.

At ideally low frequencies the sound wave increases the translational temperature by ΔT at each peak compression. Hence the population of the excited state is increased by ΔN_1, since

$$C_i \cdot \Delta T = E \cdot \Delta N_1 \quad \ldots\ldots\ldots (17),$$

where C_i is the vibrational heat capacity. For a sine wave,

$$\Delta N_1 = A \exp(i\omega t) \quad \ldots\ldots\ldots (18).$$

At ideally high frequencies the sound wave passes through the gas without substantial alteration of N_1. At intermediate frequencies, however, the population of N_1 is increased at peak compression by an amount ΔN_1^{ω} which is less than ΔN_1 and depends on ω, the angular frequency. The difference between ΔN_1 and ΔN_1^{ω} decreases with time, and using (15) we may write:

$$\frac{d(\Delta N_1 - \Delta N_1^{\omega})}{dt} = \frac{\Delta N_1 - \Delta N_1^{\omega}}{\tau}$$

which gives $\frac{d\Delta N_1^{\omega}}{dt} = \frac{\Delta N_1^{\omega}}{\tau} = \frac{A \exp(i\omega t)}{\tau}$ by (18).

Integration of this equation gives

$$\Delta N_1^{\omega} = \frac{\Delta N_1}{1 + i\omega\tau} \quad \ldots\ldots (19)$$

From (17), since ΔT and E are constants, $\frac{C_i}{C_i^{\omega}} = \frac{\Delta N_i}{\Delta N_i^{\omega}}$, giving the vibrational heat capacity at any frequency ω as

$$C_i^{\omega} = \frac{C_i}{1 + i\omega\tau} = \frac{C_0 - C_{\infty}}{1 + i\omega\tau} \quad \ldots\ldots (20)$$

where C_0 = total heat capacity, C_{∞} = heat capacity excluding vibration. The effective total heat capacity at frequency ω is thus

$$C_{\omega} = C_{\infty} + \frac{C_0 - C_{\infty}}{1 + i\omega\tau} \quad \ldots\ldots (21)$$

Now $V^2 = \frac{RT}{M}\left(1 + \frac{R}{C_V}\right)$ ..... (1)

$$= \frac{RT}{M}\left[1 + \frac{R(1 + i\omega\tau)}{C_0 + C_\infty i\omega\tau}\right]$$

The real part of this equation gives the phase velocity at frequency ω as

$$V_\omega^2 = \frac{RT}{M}\left[1 + R\left(\frac{C_0 + C_\infty \omega^2 \tau^2}{C_0^2 + C_\infty^2 \omega^2 \tau^2}\right)\right] \quad \text{..... (22)}$$

At very low frequencies ($\omega\tau \ll 1$) the velocity is given by

$$V_0^2 = \frac{RT}{M}\left[1 + \frac{R}{C_0}\right] \quad \text{..... (23)}$$

At high sound frequencies ($\omega\tau \gg 1$) the velocity is given by

$$V_\infty^2 = \frac{RT}{M}\left[1 + \frac{R}{C_\infty}\right] \quad \text{..... (24)}$$

Rearranging (22) using (23) and (24) gives the equation of the dispersion curve:

$$\omega^2\tau^2 = \frac{C_0^2}{C_\infty^2} \cdot \frac{V_\omega^2 - V_0^2}{V_\infty^2 - V_\omega^2} \quad \text{..... (25)}$$

The inflection point of this curve occurs at

$$\omega^1 = \frac{1}{\tau} \cdot \frac{C_0}{C_\infty}$$

and thus the relaxation time is given by

$$\tau = \frac{1}{2\pi f^1} \cdot \frac{C_0}{C_\infty} \quad \text{..... (26)}$$

where f^1 is the sound frequency at the inflection point at one atmosphere pressure.

τ is the relaxation time for the whole of the vibrational specific heat. There are both experimental and theoretical grounds for believing that energy is transferred to a molecule through the mode of lowest frequency, and

that it then spreads very rapidly to the other vibrational modes. The relaxation time for translational-vibrational energy transfer involving the lowest mode, β , is related to the overall relaxation time, τ , by

$$\tau = \beta \cdot \frac{C_{vib}}{C_1^*} \qquad \text{..... (27)}$$

where C_{vib} is the whole vibrational specific heat and C_1^* is that of the lowest mode.

CHAPTER 3

EXPERIMENTAL

1. INTRODUCTION

The measurements of the relaxation times were made by measuring the dispersion of ultrasound in an acoustic interferometer. The first significant measurements of sound velocity in a gas with a relaxing heat capacity were made by Pierce[2] in 1925. He used a piezo-electric transducer and a polished reflector plate which could be moved towards the transducer. He measured the velocity of sound in carbon dioxide, and showed that it increased with increasing frequency. In the 1930's several schools of ultrasonic physics came into operation. Notable among these were the schools of Pielemeier, Hubbard and Richards in the U.S.A. and that of Eucken in Germany. They used ultrasonic velocity measurements to determine relaxation times in gases and gas mixtures. All measurements of the dispersion of sound in gases have been made using the Pierce type of ultrasonic interferometer.

2. THEORY OF THE INTERFEROMETER.

The interferometer consists of an X-cut quartz crystal silvered on two opposite faces and connected to an electric oscillator. An optically flat plate is suspended above the crystal and adjusted to be accurately parallel to its upper surface. This plate is moved up or down slowly by a micrometer screw. The crystal is made to execute forced vibrations by the oscillator, but if the oscillator frequency is adjusted until it is the same as the natural resonance frequency of the crystal, the latter oscillates

with larger amplitude and generates sound waves of the same frequency as its vibrations. These sound waves travel upwards from the crystal and are reflected by the plate 180° out of phase. If the reflector is situated exactly an integral number of half wavelengths from the crystal, the initial pressure condensations from the transducer will be exactly in phase with the pressure condensations of the reflected wave, and the excess pressure on the crystal will be a maximum. At any other distance of the reflector from the crystal, the reflected wave and the pressure condensations will not be 180° out of phase with the primary wave, and the excess pressure on the transducer will be less than that in the exact resonance position.

The square of the excess pressure P gives a measure of the pressure amplitude of the transducer. Pielemeier[3] has calculated this pressure amplitude assuming perfect reflection and plane waves, and obtained a plot of P^2 against reflector distance showing sharp maxima and long flat troughs (Fig. 2).

FIG. 2

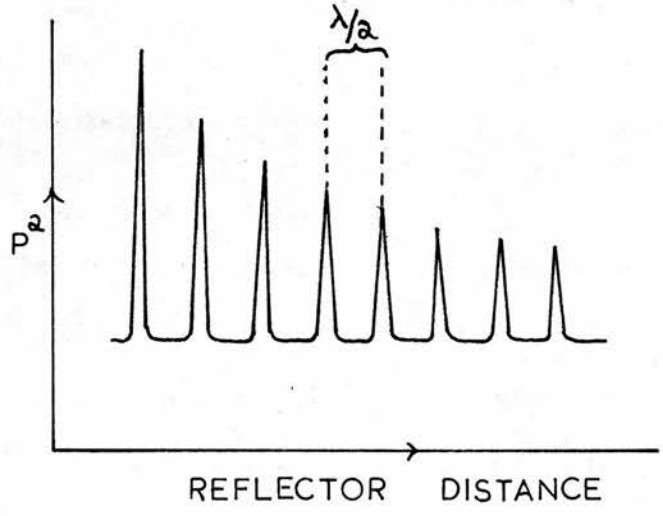

The pressure variations alter the impedance of the crystal and gas column, and this alters the anode current in the oscillator. A plot of anode

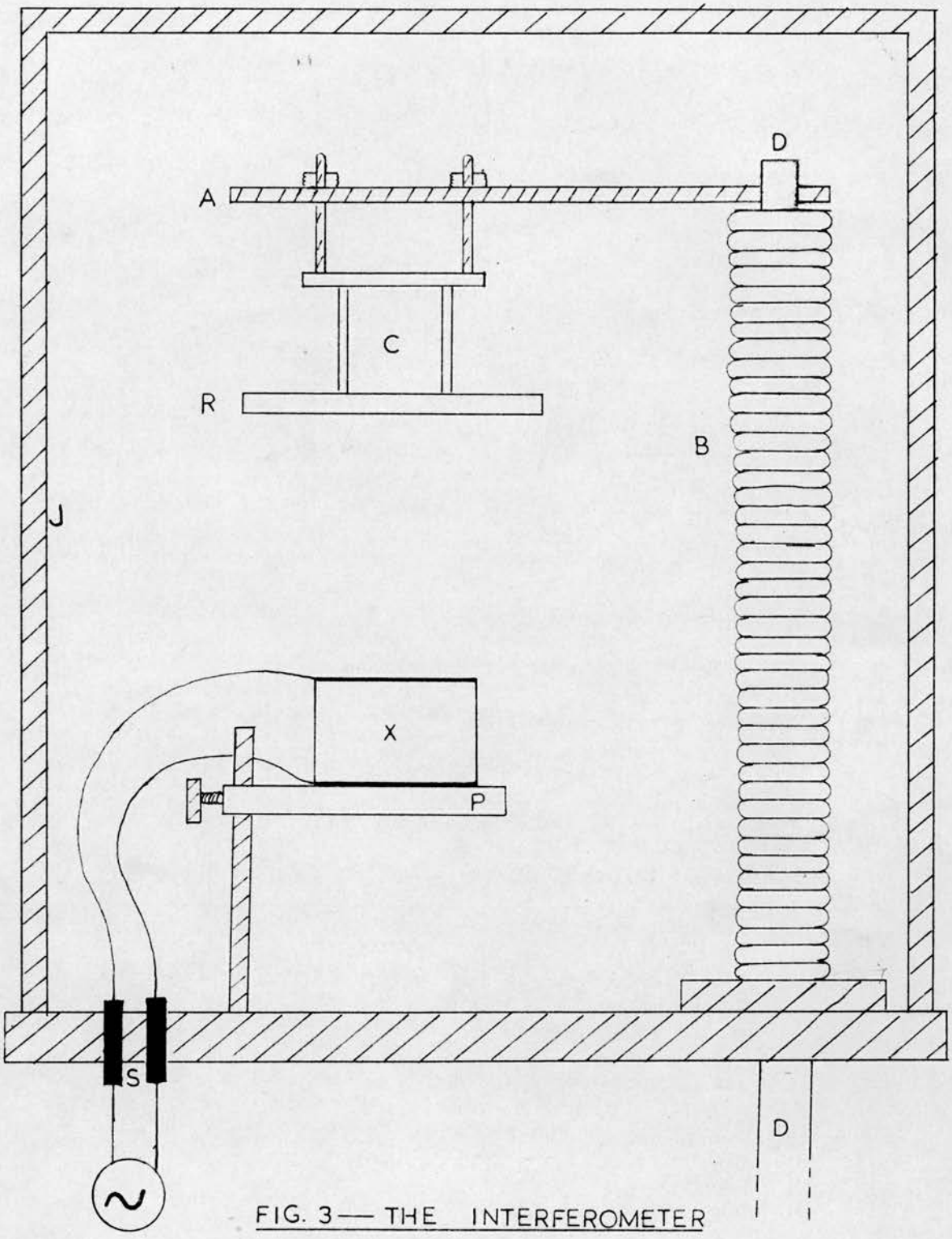

FIG. 3 — THE INTERFEROMETER

current against distance of reflector from the crystal gives a curve very similar to that of Fig. 2. The wavelength of sound can then be accurately determined by measuring the distance of travel between these peaks which are exactly $\lambda/2$ apart.

3. DESCRIPTION OF THE PRESENT INTERFEROMETER.

The construction of the present interferometer is shown in Fig. 3. The quartz crystal X sits freely on a rough glass plate P, and connection to the oscillator is made through two vacuum seals S. The optically flat glass reflector plate R is attached to the top of the driving rod D by a hollow glass cylinder C one inch long which served to eliminate any drift in the recorder base line due to capacitance effects when the crystal approaches the steel supporting arm A. This rod is attached to a metal bellows B some 15 cm long which allows the drive to enter the evacuated chamber. The rod D passes through a precision bearing in the stainless steel base of the interferometer, and is driven up and down by a micrometer-screw, connected through a reduction gear to an electric motor. The interferometer is enclosed in a cylindrical stainless steel jacket J of internal height 25 cm and internal diameter 10.0 cm. Water circulates round the interferometer at a temperature maintained constant to $\pm$ 0.01°. The absolute value of this temperature was checked against a thermometer calibrated at the National Physical Laboratory.

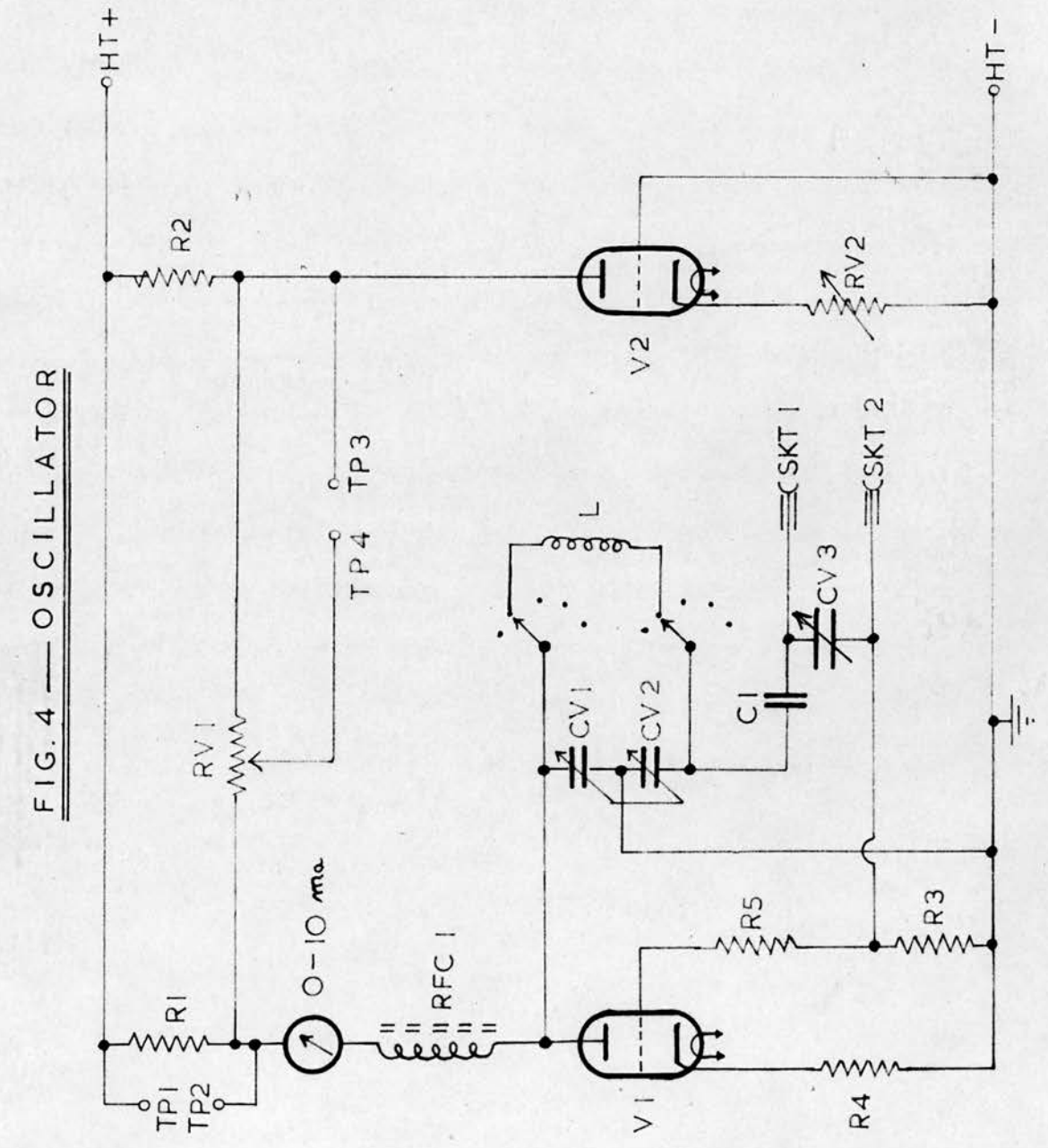

FIG. 4 — OSCILLATOR

R 1	10Ω
R 2	10Ω
R 3	47 KΩ
R 4	3·4 KΩ
R 5	22 KΩ
RV 1	1 KΩ POT. RECORDER SENSITIVITY
RV 2	5 KΩ POT. OUTPUT BALANCE
V1 & V2	12 BH 7
RFC 1	18 mH
C 1	0·001 μF 600 V
CV 1	500 pF TUNING CAPACITOR
CV 2	1000 pF TUNING CAPACITOR
CV 3	150 pF FEEDBACK CONTROL
TP1 TP2	"BLIP" INPUT
TP3 TP4	OUTPUT TO RECORDER
SKT1 SKT2	CRYSTAL SOCKETS
L	COILS

4. ELECTRONIC SYSTEM AND RECORDING.

The crystal was driven by an oscillator of frequency range $40^{kc}/s$ to $6^{mc}/s$ (Fig. 4).

It is a conventional Colpitts oscillator modified to allow controlled feedback via CV3. The natural frequency of resonance is $f = \frac{1}{2\pi\sqrt{L.\frac{CV1.CV2}{CV1+CV2}}}$. It is partly self biased by the normal leaky grid method and also by the 3.4K bias resistor in the cathode. The feedback voltage is developed across CV2 and is coupled via C1 and CV3 to appear between the grid and cathode across resistor R3. When the crystal is connected and the circuit tuned to the crystal resonance frequency, the crystal comes into the series resonant state and its impedance is at a minimum. This effectively shunts CV3, and increased feedback, and this change is indicated by a dip in the anode current meter of V1 due to the changed bias conditions caused by the increased feedback. Under working conditions RV2 is adjusted so that the grid bias of V2 allows equal currents to flow through V1 and V2. The two valves together with R1 and R2 form a Wheatstone Bridge (Fig. 5) and when the bridge is balanced A and B are at equal potentials and no current passes through RV1. Changes in the crystal impedance unbalance this bridge due to V1 acting as described and the voltage across RV1 varies accordingly.

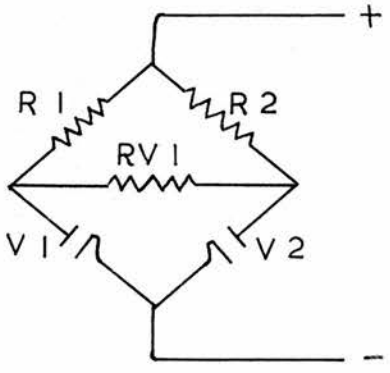

FIG. 5

The crystal was found to operate most stably with the oscillator tuned a few cycles to the fast side of the resonance dip. In an initial experiment the crystal was driven at a number of voltages between 40 and 200 volts. The sensitivity of the apparatus increased with increasing voltage, but at the higher voltages the crystal was unstable on its mounting plate. There was no variation of the observed wavelength with voltage in this range, showing that the velocity of sound is independent of the sound intensity here. A working voltage of 120V gave maximum sensitivity with no instability, and this was used throughout.

A suitable fraction of the potential drop across RV1 was fed to a Honeywell-Brown fast recording potentiometer. The recorder chart thus showed a trace similar to Fig. 2 on which the distance between each successive maximum was proportional to half the wavelength of sound in the gas under investigation. The distance scale of the chart was calibrated by arranging for the micrometer screw which drove the reflector to depress a micro-switch once in every revolution. This short-circuited R1 (Fig. 4), unbalanced the Wheatstone bridge network, and superimposed a series of sharp blips on the recorder chart, the distance between any two blips being proportional to the pitch of the micrometer screw. From this pitch the half-wavelength of sound in the gas should be obtainable by simple proportion assuming that ths speeds of the driving motors for both the recorder chart and the reflector remain constant.

5. CORRECTION FOR NON-LINEARITY OF THE RECORDER CHART AND CALCULATION OF $\lambda/2$.

Unfortunately this latter assumption was not valid as the speed of the motor driving the reflector was found to vary slightly with time. This variation was never large, but it led to a random inaccuracy of

one or two parts per thousand in the observed wavelength. A small correction was made for this non-linearity of the chart as follows.

Consider a distance x on the recorder chart. Let n_b be the number of calibration blips in this distance and n_p the number of peaks. Let b be the true separation of the blips on the recorder chart and p the true separation of the peaks. Then if the chart is linear

$$\frac{n_b}{n_p} = \frac{p}{b} = \frac{\lambda/2}{\text{Pitch of micrometer screw}} \quad \ldots\ldots (28)$$

If the chart is not linear this relation no longer holds and a correction must be applied. Then

$$x = b.\, n_b + \Delta b(x) + c$$

$$\text{and } x = p.\, n_p + \Delta p(x) + d.$$

where $\Delta b(x), \Delta p(x)$ are the deviations from linearity of blips or peaks at the point x on the chart, and c and d are constants. Thus

$$n_b = \frac{x - \Delta b(x) - c}{b} \quad \text{giving}$$

$$\frac{dn_b}{dx} = \frac{1}{b}\left[1 - \frac{d}{dx}\Delta b(x)\right]$$

Similarly $$\frac{dn_p}{dx} = \frac{1}{p}\left[1 - \frac{d}{dx}\Delta p(x)\right]$$

Thus $$\left(\frac{dn_b}{dn_p}\right)_x = \frac{p}{b}\,\frac{\left[1 - \frac{d}{dx}\Delta b(x)\right]}{\left[1 - \frac{d}{dx}\Delta p(x)\right]}$$

$$= \frac{p}{b}\left[1 - \frac{d}{dx}\left\{\Delta b(x) - \Delta p(x)\right\}\right] \quad \ldots\ldots (29)$$

At a number of points along the chart, therefore, the deviations from linearity of both peaks and blips were estimated graphically giving $(\Delta b - \Delta p)$ at

each point. The gradient of the plot of $(\Delta b - \Delta p)$ against x then gave the required correction factor.

The pitch of the micrometer screw was measured to 1 in 3000 using an accurate cathetometer and checked against another cathetometer. The value obtained was 0.06320 ± 0.00002 cm. This was checked at intervals for wear or irregularity but showed no variation. After a correction had been made for non-linearity of the chart, $\lambda/2$ could be calculated from this value of the pitch. Reproducibility from run to run was better than 1 in 1200.

6. CRYSTALS AND FREQUENCY MEASUREMENT.

The X-cut quartz crystals used as transducers would oscillate most stably with only a very fine film of silver on their faces. They were cleaned with concentrated nitric acid, degreased with alcoholic KOH, and washed thoroughly with distilled water. Slow silvering for one minute by a modified version of Brashear's[4] process gave a suitable film. Fine platinum leads were attached to the silvered surface using a mixture of Devcon aluminium putty (75%) with copper dust (25%) to make it conducting. The frequencies of the crystals were measured to 1 in 5000 by loose coupling to an LM-14 frequency meter standardised against the B.B.C. Light programme.

7. PARALLELISM OF THE REFLECTOR.

One of the most important conditions for the accurate measurement of the velocity of sound in an interferometer is that the surfaces of the crystal and of the reflector plate should be absolutely parallel. The effect of non-parallelism is shown in Fig. 6. The crystal and reflector were made parallel to within ten microns using metal feelers, and the wavelength of sound was measured in this position and in various positions of non-parallelism.

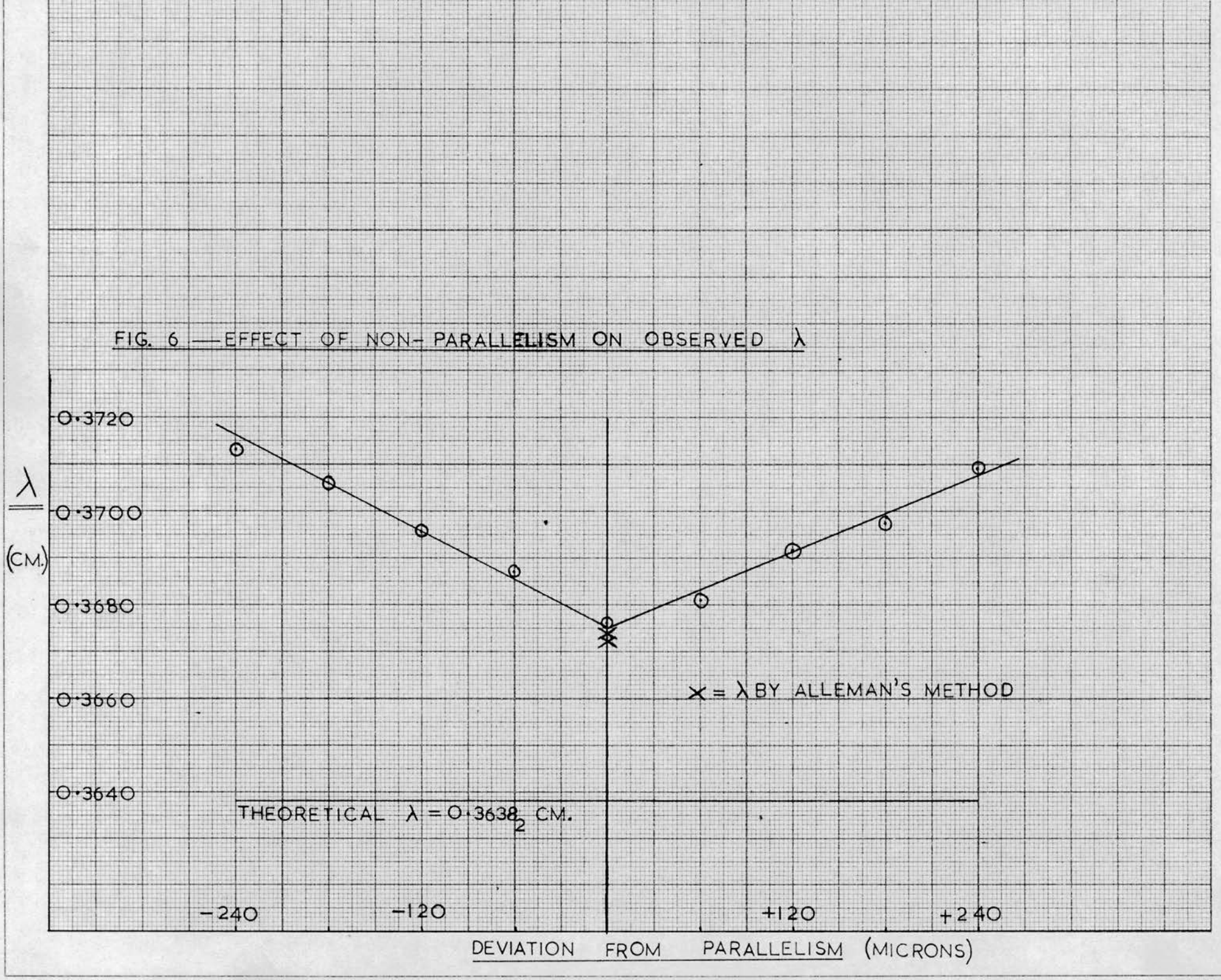
FIG. 6 — EFFECT OF NON-PARALLELISM ON OBSERVED λ
λ
(CM.)
0·3720
0·3700
0·3680
0·3660
0·3640
× = λ BY ALLEMAN'S METHOD
THEORETICAL λ = 0·3638 CM.
2
−240
−120
+120
+240
DEVIATION FROM PARALLELISM (MICRONS)

The observed wavelength was a minimum in the position of best parallelism. This position is best attained while the interferometer is in operation by the method described by Alleman[5]. When the reflector and crystal surface are not parallel, a number of secondary peaks appear. The inclination of the reflector is altered until the secondary peaks disappear, and then adjusted to give maximum peak height. The method is very sensitive to small displacements of the reflector, and it was employed for all adjustments. When the wavelength of sound was measured under these conditions it was the same as that obtained in the position of best parallelism using feelers.

8. TRANSVERSE WAVE CORRECTION.

The wavelength of sound under these conditions, corrected by eqn. 12 for gas imperfection only, is greater than that calculated from the thermodynamic properties of the gas. The crystal is not vibrating as a perfect piston to produce a plane wave, but is instead vibrating in a complex mode to give a cylindrically symmetrical wave of wavelength longer than that of the pure plane wave. The relationship between the observed wavelength and the plane wavelength is given by[6]:

$$k_n = k \left[1 - \frac{x_n}{kb} \right]^{\frac{1}{2}} \quad \ldots\ldots\ldots (30)$$

where k_n is the propagation constant ($= \frac{2\pi}{\lambda}$) of the n^{th} Rayleigh mode, k is the plane wavelength, x_n is the root of the Bessel function for this n^{th} mode of the wave motion, and b is the internal radius of the interferometer chamber. A plot of the relative error in the wavelength against the square of the calculated wavelength should thus be a straight line,[7,8] from which the appropriate correction may be applied to the observed wavelength.

The present interferometer was calibrated with dry, carbon dioxide-free air or nitrogen. The calibrations for any one crystal lay on a straight line at different temperatures, but a different line was obtained from a different crystal. The correction is about 1 in 200 at 87 $^{kc}/_{s}$ but only 1 in 1000 at 227 and 694 $^{kc}/_{s}$, being largest in methane where the wavelength is long. The dispersion curves obtained with crystals of different frequencies agree closely, and this confirms the accuracy of the transverse wave corrections.

9. VACUUM SYSTEM.

This was of conventional design, constructed of Pyrex glass. The system was evacuated through a liquid nitrogen trap by an electrically heated mercury diffusion pump backed by a rotary oil pump. When thoroughly degassed, the interferometer chamber held a vacuum of less than one micron of mercury for an hour. The pressure of gas in the interferometer was measured on a U-tube mercury manometer which read to two atmospheres.

10. THE CLUSIUS-RICCOBINI FRACTIONATION COLUMN.

Because of the large catalytic effect of certain impurities on the efficiency of energy transfer, it is necessary to prepare gases of the highest possible purity. Although conventional freezing and distillation in cold traps is sometimes adequate, this method will not separate gases unless their boiling points differ considerably nor will it remove small quantities of air from methane. Two possible methods of gas purification were considered: preparative scale gas chromatography and low temperature fractional distillation. The former suffers from the disadvantage that it may introduce some small unsuspected contaminant from the carrier gas and

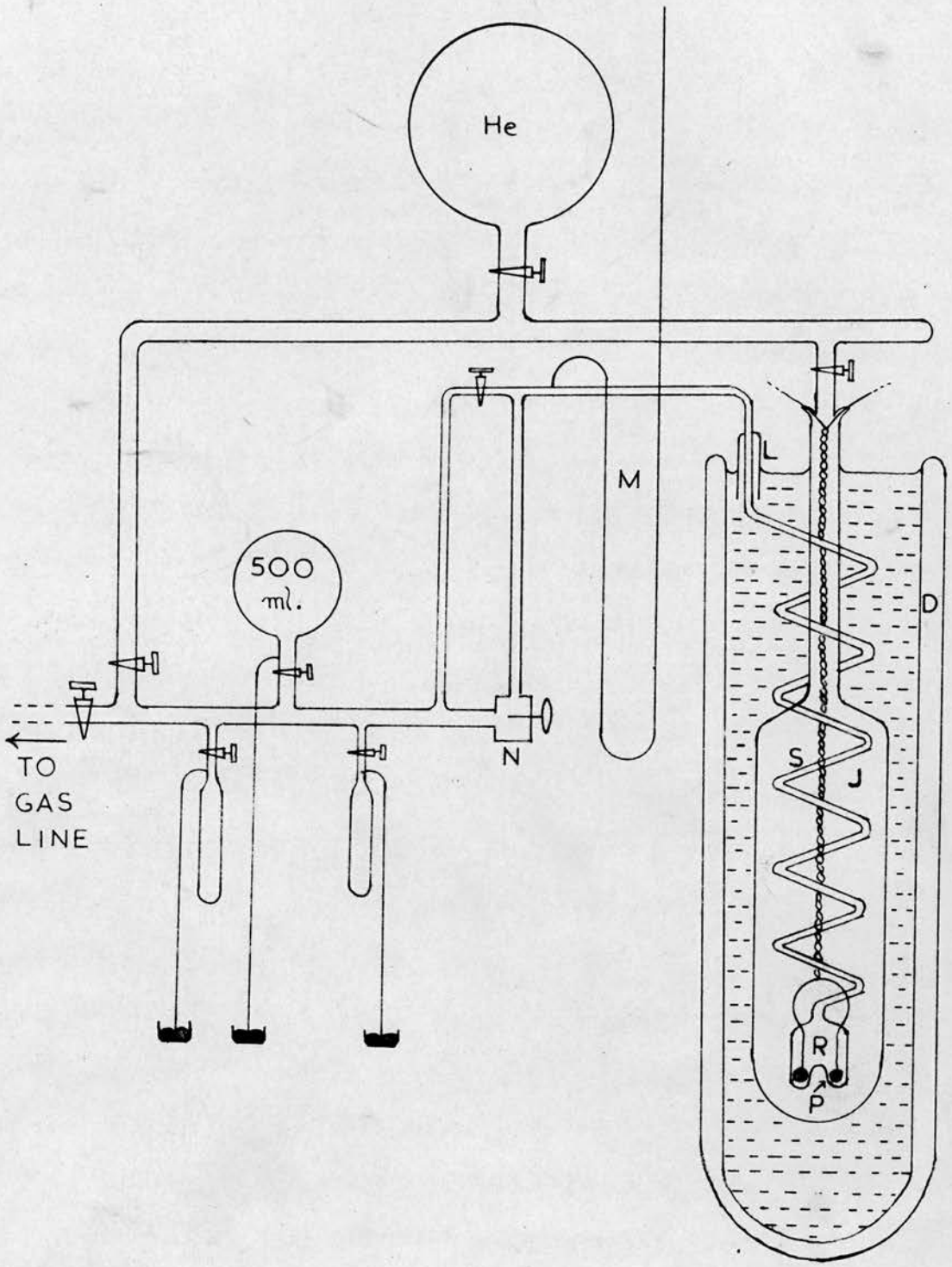

FIG. 7 — FRACTIONATION COLUMN

that appreciable hydrogen exchange may take place with deuterated compounds. The latter alternative was therefore adopted.

Fig. 7, which is not drawn to scale, shows the low temperature fractionation column which is a modified version of that described by Clusius and Riccobini[9]. The method of operation was as follows.

Helium at about 3 cm. pressure was allowed into the outer jacket J of the column and the Dewar flask D filled with a suitable coolant (e.g. liquid oxygen) to a level a few inches above the foot of this jacket. The gas to be purified was admitted to the spiral S, and it condensed into the reservoir R. When all the gas had condensed, the helium in the outer jacket was pumped away leaving the condensed gas thermally insulated. The Dewar vessel was filled, and the level of the coolant was maintained above the constant level tube L so that the same length of the column was always in contact with the coolant. A suitable current was passed through a spiral of platinum wire P in the base of the reservoir and the liquid refluxed gently. When equilibrium was reached (ca. 1 hour) the gas was bled off (ca. 1 litre in 2 hours) through the needle valve N and condensed, its pressure being noted on manometer M. When all high boiling impurities had distilled off, the manometer fell rapidly to the vapour pressure of the pure gas at the temperature of the coolant, and remained there until all this gas had distilled, when it fell rapidly again. Only the middle fraction of the distillate was collected. The vapour pressure indicated clearly which gas was being distilled at any moment, and subsequent analysis showed that clean separating had been obtained.

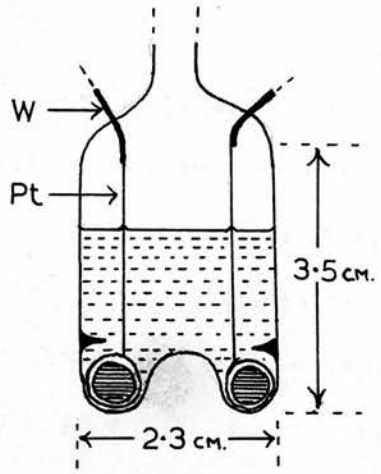

FIG. 8

Fig. 7 gives most of the constructional details, and Fig. 8 shows the construction of the reservoir. The platinum spiral, 0.15 mm. in diameter and 50 cm. long, is wound on a glass ring and is "hard soldered" to thick pieces of tungsten wire where it leaves the reservoir. The spiral was heated by maintaining a constant voltage of 1.0 V across it from an accumulator and rheostat.

The Dewar vessel in which the column was immersed, internal diameter 9.5 cm, depth 70 cm, was made of heavy Pyrex tubing with an annular space of 8 mm between the inner and outer tubes. During construction the two tubes were held rigidly by tightly packed copper gauze while they were joined at the lip of the vessel. Three balls of asbestos string were then carefully packed between the two tubes. The copper gauze was dissolved in dilute nitric acid and the vessel cleaned thoroughly with alcoholic KOH and distilled water before silvering[4]. Finally the interior of the vessel was evacuated for several days.

CHAPTER 4

MATERIALS

1. AIR. Air was prepared free from carbon dioxide and water vapour by passing it slowly through the purification train shown in Fig. 9.

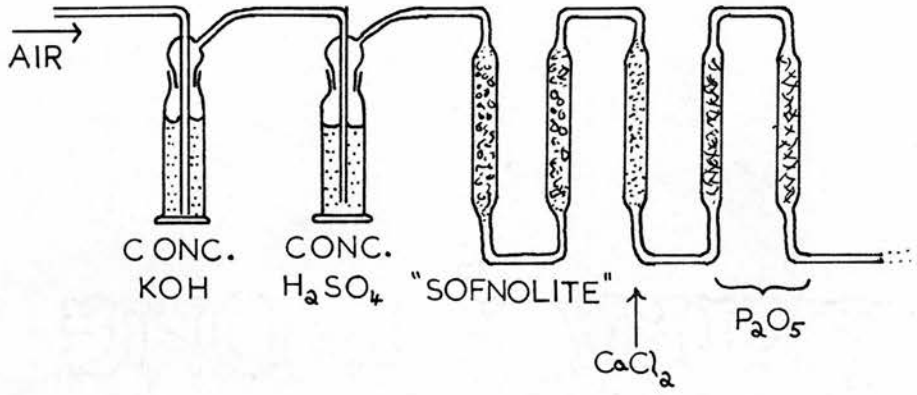

FIG. 9 — AIR PURIFICATION TRAIN

2. NITROGEN. This was obtained from a cylinder containing 99.9% nitrogen and 0.05% oxygen. The gas was passed slowly over "sofnolite" to remove carbon dioxide, heated copper powder to remove oxygen, heated copper oxide to remove hydrogen, and dried by phosphorus pentoxide. The inert gas content (mostly neon) was stated to be not more than 1 in 1500.

3. METHANE. Three samples of methane were used:

(i) Two litres of gas "containing no detectable impurities" were obtained from Twentieth Century Electronics, Ltd. Gas chromatographic analysis showed that less than 0.01% of ethane or higher hydrocarbons or 0.05% of air could be present.

(ii) A second sample was prepared by Grignard reduction of methyl magnesium iodide with water using the apparatus shown in Fig. 10.

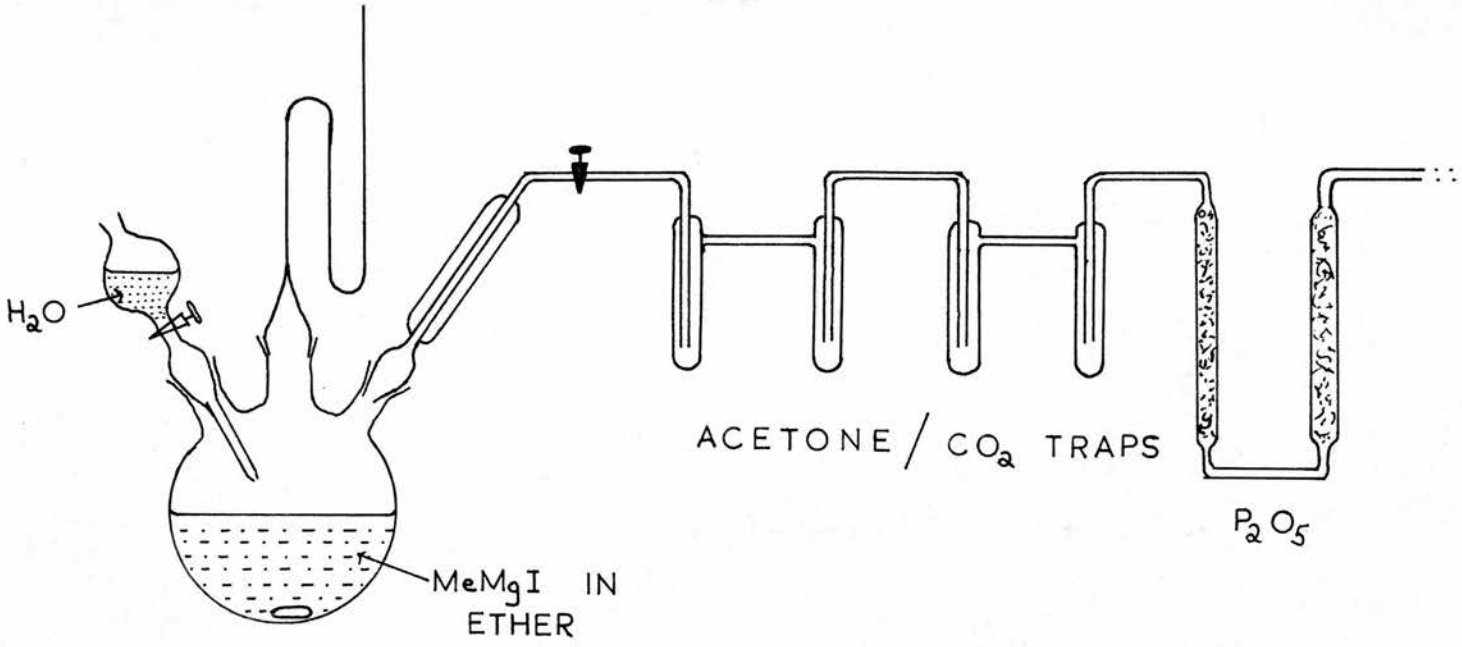

FIG. 10 — GAS PREPARATION LINE

To 15 g. clean magnesium turnings and 200 ml. dry, peroxide-free, redistilled di-n-butyl ether in a 500 ml. round-bottomed flask was added slowly 30 ml. of dry, redistilled methyl iodide in 100 ml. di-n-butyl ether. The mixture was maintained at 70° with magnetic stirring, and then refluxed for a short time to complete the reaction. About 30 ml. of distilled water were added slowly, and the methane evolved was passed through four acetone/CO_2 traps and phosphorus pentoxide before condensing in liquid nitrogen. The methane was fractionated in the Clusius-Riccobini column. Gas chromatographic analysis on a Linde molecular sieve, five feet long, 4 mm internal diameter, and 40-60 mesh, using hydrogen as a carrier gas, showed no detectable impurities within the limits given above. The yield of pure methane was about five litres at N.T.P.

(iii) A third sample was prepared from commercial cylinder methane containing about 95% CH_4. A stream of this was passed through four acetone/CO_2 traps and phosphorus pentoxide, and part of the methane stream condensed in a liquid oxygen trap. The liquid methane was frozen solid in liquid nitrogen, the supernatant vapour pumped away, and the process repeated

several times to remove as much air as possible. The methane was finally fractionated in the Clusius-Riccobini column, and no impurities could be detected within the above limits.

The vapour pressure of all three methane samples was 8.3 cm. at -183.1°.

4. TETRADEUTEROMETHANE. This was prepared from aluminium carbide and heavy water (Norsk Hydro-Elektrisk; 99.99 g. D_2O per 100 g.; $d_4^{20} = 1.1054$). 20 g. of aluminium carbide were heated under high vacuum at 600°C in a Pyrex glass tube for 96 hours. This removed all water and adsorbed hydrogen and decomposed all hydroxides except sodium and potassium hydroxides. The aluminium carbide was placed in a 500 ml. round-bottomed flask and 30 ml. of deuterium oxide placed in a dropping funnel, both these operations and the filling of the phosphorus pentoxide drying tubes being performed in a glove chamber filled with dry air. The system was evacuated for 48 hours, and flamed lightly at intervals. These strict precautions were taken to eliminate any trace of hydrogen from the system. After adding the deuterium oxide to the aluminium carbide, the flask was warmed slowly, and tetradeuteromethane was evolved briskly at 80°. It was passed through acetone/CO_2 traps and phosphorus pentoxide and condensed in liquid nitrogen. The gas was then fractionated in the Clusius-Riccobini column. The yield of purified gas was 4.5 l, and the vapour pressure at -183.1° was 8.9 cm. Gas chromatographic analysis showed that less than 0.01% of ethane or higher hydrocarbons or 0.05% of air could be present, and no other impurities were detected. Infra-red analysis on a Hilger H800 spectrometer showed no detectable CH_4, i.e. no more than 0.5% of CH_4 was present.

5. SILANE. Silane, SiH_4, was prepared by reduction of silicon tetrachloride with lithium aluminium hydride in di-n-butyl ether as solvent. The ether was freed from peroxides, distilled and dried over sodium. 13 g. of lithium aluminium hydride were placed in a dry 500 ml. round-bottomed flask equipped with a magnetic stirrer, and the system evacuated for 48 hours to remove all traces of oxygen. 150 ml. of di-n-butyl ether were then added, and stirred until the lithium aluminium hydride dissolved. 120 g. of dry, redistilled silicon tetrachloride in 150 ml. di-n-butyl ether were added dropwise with with stirring. Silane was evolved instantaneously, and, in the absence of oxygen, smoothly. It was dried and separated from ether vapour by passing through four acetone/CO_2 traps and phosphorus pentoxide, and condensed in liquid nitrogen. The solid was melted, refrozen and pumped several times, and then distilled three times from one cold trap to another. The yield was five litres at N.T.P., with zero vapour pressure at -196°C. The molecular weight determined by the method of limiting densities was (32.05 $\pm$ 0.04) compared with a theoretical molecular weight of 32.12. Infra-red analysis showed no detectable impurities.

6. TETRADEUTEROSILANE. This was prepared by reduction of silicon tetrachloride with lithium aluminium deuteride (Metal Hydrides, Inc.) in ether. To obtain as large a yield as possible from the 5 g. of lithium aluminium deuteride available, di ethyl ether was used as solvent in place of di-n-butyl ether, although its vapour pressure was inconveniently high at room temperature. The ether was distilled twice in anhydrous conditions and dried with sodium. The silicon tetrachloride was distilled twice in anhydrous conditions and dried with calcium chloride. The drying tubes were filled with fresh phosphorus pentoxide in a glove chamber filled with dry nitrogen, and the preparation line evacuated and flamed for 48 hours.

100 g. of silicon tetrachloride in 150 ml. ether were added to the flask. The 5 g. of lithium aluminium deuteride were dissolved in 150 ml. ether in the glove chamber, and dropped slowly into the flask with stirring. The tetradeuterosilane was evolved smoothly at once. The mixture was finally refluxed for a short time to complete the reaction. The gas was dried and distilled in the same way as was silane. The yield of pure gas at N.T.P. was some 2.2 l., only about 60% of the theoretical yield. It had zero vapour pressure at -196°, and infra-red analysis showed that less than 0.5% of silane was present. The molecular weight by the method of limiting densities was 36.07 ± 0.04 compared with the theoretical 36.15.

Care was necessary in handling the silanes as they were oxidised violently by air. When a small amount of silane was pumped into the atmosphere, the intensity of the flame produced was comparable to that of magnesium burning in air.

CHAPTER 5

CALCULATION OF THE THEORETICAL VALUES OF THE VELOCITY OF SOUND

The velocity of sound in an ideal gas is

$$V = \sqrt{\left(1 + \frac{R}{C_v}\right) \frac{RT}{M}} \qquad \ldots\ldots\ldots\ldots\ldots (1)$$

The translational and the rotational modes each contribute $\frac{3}{2}$ R to the heat capacity C_v of the tetrahedral hydrides. The limiting value of the velocity of sound at high frequencies is thus

$$V = \sqrt{\frac{4RT}{3M}} \qquad \ldots\ldots\ldots\ldots\ldots (24)$$

At low sound frequencies the molecular vibrations also contribute to the molecular heat capacity. The frequencies ν of the various modes are obtained from spectroscopic observations, and the contribution C_ν of each vibration to the vibrational heat capacity is given by the Planck-Einstein formula

$$\frac{C_\nu}{R} = \left(\frac{h\nu}{kT}\right)^2 \times \frac{e^{h\nu/kT}}{\left(e^{h\nu/kT} - 1\right)^2} \qquad \ldots\ldots (31)$$

The sum of terms like those in eqn. 31 for every fundamental and every degeneracy gives the vibrational heat capacity. But the higher the frequency of a mode, the smaller is its contribution to the vibrational heat capacity, and thus modes with frequencies greater than 3000 $cm.^{-1}$ may generally be neglected. The heat capacity at low sound frequencies is thus $3R + \Sigma C_\nu$, and the velocity of sound is obtained from eqn. 23.

1. AIR. The velocity of sound in dry, carbon dioxide-free air was calculated from the known composition of air (78.03% nitrogen, 20.99% oxygen and 0.98% argon) and from the calculated values of the heat capacities of nitrogen[10], oxygen[11], and argon. This assumes no vibrational contribution to the heat capacities, and gives

$$V_{id} = 346.1_6 \text{ m/s at } 25^\circ\text{C}; \qquad V_{id} = 373.7_7 \text{ m/s at } 75^\circ\text{C}$$

for the ideal gas state. As the composition of air is not constant to more than 0.05%[12], the accuracy of these velocities cannot be greater than 1 in 2000. A small correction for gas imperfection is applied to the observed velocities using the virial data of Holborn and Otto[13]:

$$V_{obs} = V_{id} (1 + 3.6\ p \times 10^{-6}) \text{ at } 25^\circ\text{C}.$$

$$V_{obs} = V_{id} (1 + 5.7\ p \times 10^{-6}) \text{ at } 75^\circ\text{C}.$$

where p is the pressure in cm. Hg.

2. NITROGEN. The velocity of sound in nitrogen was calculated as in the case of air, and the virial correction for air applied:

$$V_{id} = 351.9 \text{ m/s at } 25^\circ\text{C}.$$

3. METHANE. All the fundamental vibrations of methane except ν_2 have been established accurately[14]. They are: $\nu_1 = 2914.2$ cm.$^{-1}$; $\nu_2 = 1520\ (\pm 20)$; $\nu_3 = 3020.3$; $\nu_4 = 1306.2$. The vibrational heat capacity is 0.576_0 and 1.094_1 cal. mole^{-1} deg.$^{-1}$ at 25°C and 75°C respectively. The velocities of sound in the ideal gas are:

$$V_0 = 448.9 \text{ m/s} \quad ; \quad V_\infty = 453.9 \text{ m/s} \quad \text{at } 25^\circ\text{C}.$$

$$V_0 = 480.9 \text{ m/s} \quad ; \quad V_\infty = 490.5 \text{ m/s} \quad \text{at } 75^\circ\text{C}.$$

The dispersion at 25°C is 5 m/s, which is only 1% of the velocity. The values of the second virial coefficient were taken from Hirschfelder, Bird and Spotz[15], and this gives

$$V_{obs} = V_{id} (1 - 8.6\ p \times 10^{-6}) \quad \text{at } 25^{\circ}C$$

$$V_{obs} = V_{id} (1 - 3.1\ p \times 10^{-6}) \quad \text{at } 75^{\circ}C$$

where p is the pressure in cm. Hg.

4. TETRADEUTEROMETHANE. The fundamentals are[14]: $\nu_1 = 2084.7$ cm.$^{-1}$; $\nu_2 = 1054\ (\pm 20)$; $\nu_3 = 2258.2$; $\nu_4 = 995.6$. The vibrational heat capacity is 1.812 and 2.770 cal. mole^{-1} deg.$^{-1}$ at 25°C and 75°C respectively. The velocities of sound in the ideal gas are:

$$V_0 = 393.8\ \text{m/s} \quad ; \quad V_\infty = 405.8\ \text{m/s} \quad \text{at } 25^{\circ}C$$

$$V_0 = 420.8\ \text{m/s} \quad ; \quad V_\infty = 438.5\ \text{m/s} \quad \text{at } 75^{\circ}C$$

No virial or critical data are available for tetradeuteromethane, and thus the correction for gas imperfection was taken to be the same as that for methane. This correction only exceeded 1 in 1000 at the highest pressures used.

5. SILANE. The fundamentals of silane have been investigated by several workers. The values taken were: $\nu_1 = 2187$ cm.$^{-1}$; $\nu_2 = 978$[16]; $\nu_3 = 2188$; $\nu_4 = 914$[17]. The vibrational heat capacity is 2.272 and 3.299 cal. mole^{-1} deg.$^{-1}$ at 25°C and 75°C respectively. The velocities of sound in the ideal gas are:

$$V_0 = 309.5\ \text{m/s} \quad ; \quad V_\infty = 320.8\ \text{m/s} \quad \text{at } 25^{\circ}C$$

$$V_0 = 330.9\ \text{m/s} \quad ; \quad V_\infty = 346.6\ \text{m/s} \quad \text{at } 75^{\circ}C$$

No virial data for the silanes are available, but the values of Stock and Somieski[18] for the critical temperature and pressure are:

$$T_c = -3.5^{\circ}C \; ; \qquad p_c = 48 \text{ atmospheres.}$$

The second virial coefficient can then be calculated approximately from the Berthelot equation for B:

$$B = \frac{9RT_c}{128\, p_c}\left(1 - 6\,\frac{T_c^2}{T^2}\right) \qquad \ldots\ldots\ldots (32)$$

At low sound frequencies this gives

$$V_{obs} = V_{id}\,(1 - 3.89 \times 10^{-5}\, p) \qquad \text{at } 25^{\circ}C.$$

$$V_{obs} = V_{id}\,(1 - 2.19 \times 10^{-5}\, p) \qquad \text{at } 75^{\circ}C.$$

where p is the pressure in cm. Hg. The value of B obtained from eqn. 32, -127 cc/mole, agrees with that obtained experimentally by the method of limiting densities, 130 ($\pm$ 15) cc/mole.

6. TETRADEUTEROSILANE. The fundamentals of tetradeuterosilane have been measured by two sets of workers. The values taken were: $\nu_1 = 1582$ cm.$^{-1}$; $\nu_2 = 689$[19]; $\nu_3 = 1597$; $\nu_4 = 675$[17]. The vibrational heat capacity is 4.551 and 5.821 cal. mole^{-1} deg.$^{-1}$ at 25°C and 75°C respectively. The velocities of sound in the ideal gas are:

$$V_0 = 285.6 \text{ m/s} \; ; \qquad V_\infty = 302.4 \text{ m/s} \qquad \text{at } 25^{\circ}C$$

$$V_0 = 305.9 \text{ m/s} \; ; \qquad V_\infty = 326.8 \text{ m/s} \qquad \text{at } 75^{\circ}C$$

No virial or critical data are available for tetradeuterosilane, and the correction applied for gas imperfection was the same as that applied to silane.

CHAPTER 6

RESULTS

The measurements were made with crystals of frequencies 86, 228, and 694 $^{kc}/s$. A decrease in pressure decreases the number of gas collisions per second, and this is equivalent to increasing the frequency of the sound wave in a dispersing gas. Thus measurements made at pressures between 130 and 15 cm. Hg covered an effective frequency range of 50 to 3000 $^{kc}/s$. The interferometer was calibrated in dry, carbon dioxide-free air or nitrogen immediately before a series of measurements in another gas. The calibrations were taken at pressures between 80 and 20 cm., but the wavelength in air of sound of any frequency did not vary with pressure.

In the calculation of the results, the ratio of the separation on the recorder chart of the half-wavelength peaks to that of the calibration blips is corrected for non-linearity of the chart by eqn. 29. When this ratio is multiplied by the pitch of the micrometer screw, 0.06320 cm., it gives the observed half-wavelength of sound. This wavelength in air, corrected for gas imperfection by eqn. 12, is $\lambda_{obs.}$ in the tables of results. The mean value of $\lambda_{obs.}$ is compared with that derived from the thermodynamic properties of air, and the relative error in the wavelength found. This gives the transverse wave correction graph for each crystal.

In the calculation of the results for the methanes and silanes, the observed wavelength is corrected for gas imperfection by eqn. 12 with the appropriate value of C_v. The transverse wave correction is

then applied to $\lambda_{obs.}$ to give $\lambda_{corr.}$, and the product $\lambda_{corr.}$ and the frequency is the velocity of sound V. V^2 is plotted against the logarithm of frequency/pressure, and the dispersion curve calculated from eqn. 25 is drawn. Since this is symmetrical, the intersection of the line $\frac{V_o^2 + V_\infty^2}{2}$ with the curve gives the point of inflection, from which the relaxation time may be calculated from eqn. 27.

Care was taken to make corresponding measurements on each pair of isotopic gases under identical conditions, so that no undetected systematic error could affect the ratio of the results for the two compounds.

1. Calibrations with Air.

(i) $85.66^{kc}/s$; 25°C.

No.	P(cm.)	$P/_b$	$\lambda_{obs.}$(cm.)
1	76	3.229_8	0.4081_4
2	76	3.230_8	0.4082_6
3	76	3.231_0	0.4082_9
4	76	3.233_2	0.4085_7
5	68	3.231_2	0.4083_3
6	56	3.229_1	0.4080_8
7	50	3.229_3	0.4081_1
8	38	3.230_4	0.4082_7
9	30	3.231_7	0.4084_4
10	20	3.230_5	0.4083_1

Theoretical $\lambda = 0.4041_1$ cm. Mean observed $\lambda = 0.4082_8$ cm.

$\frac{\Delta\lambda}{\lambda} = 0.0103$ $\lambda^2 = 0.163$ cm.^{2}

FIG. 10 — TRANSVERSE WAVE CORRECTION GRAPH — 85·7 kc/s

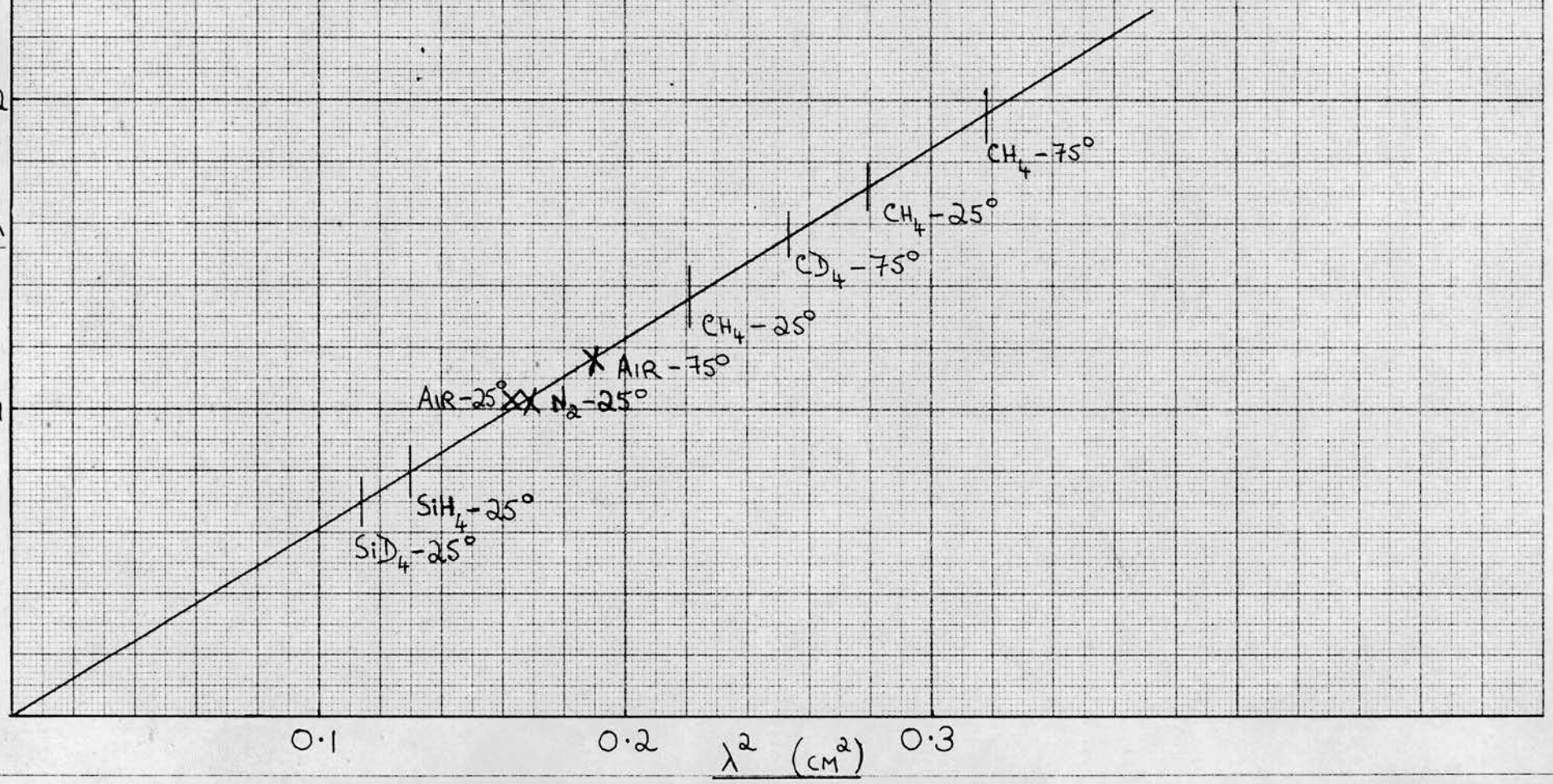

(ii) 85.75 kc/s; 75°C.

No.	P (cm.)	$p/_b$	$\lambda_{obs.}$ (cm.)
11	75	3.492_4	0.4412_5
12	75	3.489_8	0.4409_2
13	75	3.490_1	0.4409_6
14	75	3.490_0	0.4409_5
15	65	3.488_1	0.4407_4
16	54	3.490_2	0.4410_2
17	45	3.487_8	0.4407_5
18	40	3.487_4	0.4407_1
19	40	3.488_2	0.4408_1
20	33	3.491_1	0.4412_0

Theoretical $\lambda = 0.4358_8$ cm. Mean observed $\lambda = 0.4409_3$ cm.

$\frac{\Delta\lambda}{\lambda} = 0.0116$ $\lambda^2 = 0.190$ cm.^{2}

Fig. 10 is the correction graph for the transverse wave effect at 85.7 kc/s

(iii) 228.12 kc/s; 25°C.

No.	P (cm.)	$p/_b$	$\lambda_{obs.}$ (cm.)
21	73	1.202_7	0.1519_8
22	73	1.202_0	0.1518_9
23	73	1.202_3	0.1519_3
24	63	1.203_9	0.1521_3
25	53	1.204_0	0.1521_6
26	44	1.203_2	0.1520_6
27	34	1.202_2	0.1519_4
28	24	1.202_7	0.1520_1

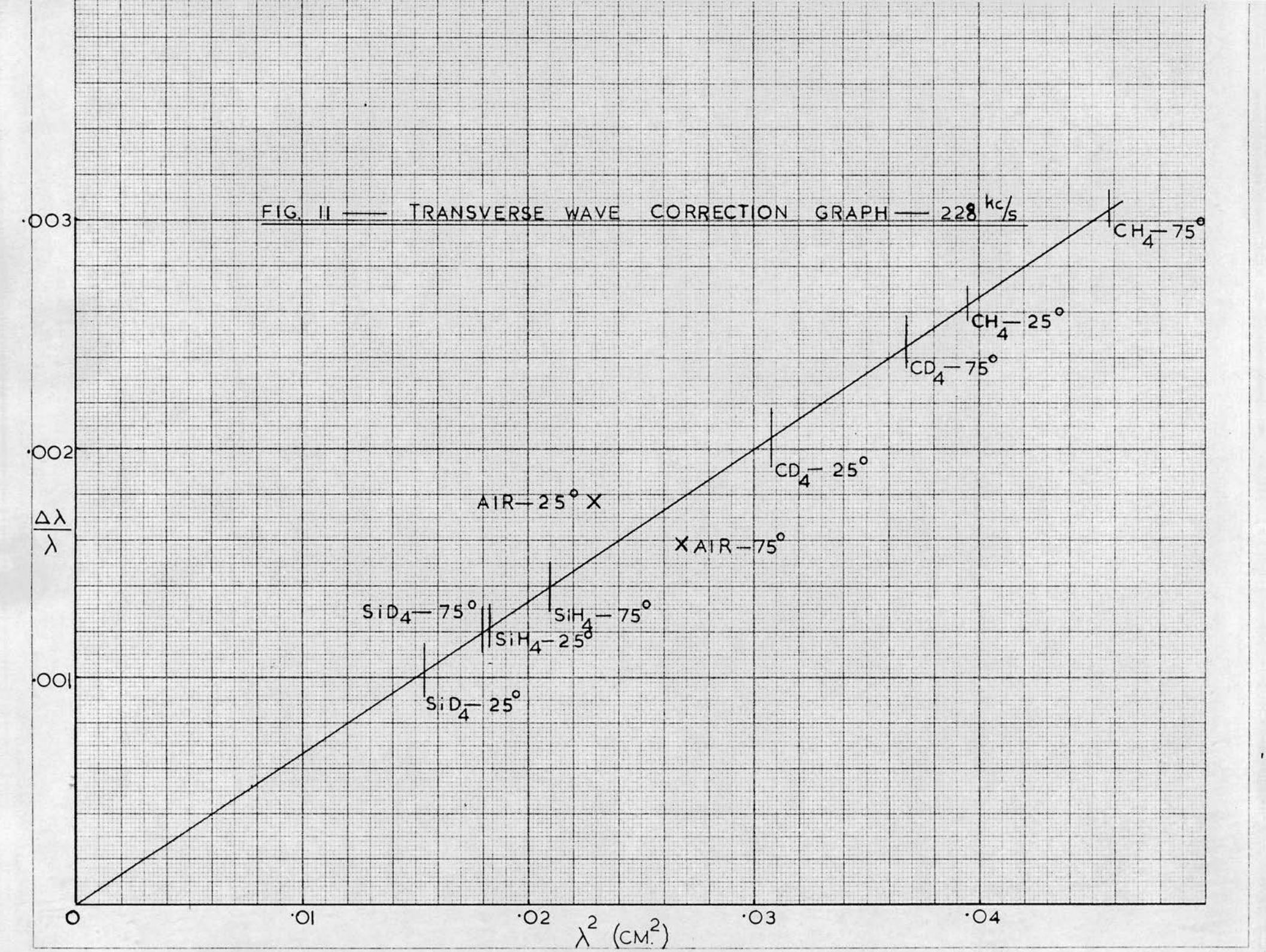
FIG. 11 —— TRANSVERSE WAVE CORRECTION GRAPH —— 228 kc/s
·003
·002
·001
0
·01
·02
·03
·04
$\frac{\Delta\lambda}{\lambda}$
λ^2 (CM.^{2})
CH_4 — 75°
CH_4 — 25°
CD_4 — 75°
CD_4 — 25°
AIR — 25°
AIR — 75°
SiD_4 — 75°
SiH_4 — 75°
SiH_4 — 25°
SiD_4 — 25°

Theoretical $\lambda = 0.1517_4$ cm. Mean observed $\lambda = 0.1520_1$ cm.

$\frac{\Delta\lambda}{\lambda} = 0.0017_8$ $\lambda^2 = 0.0230$ cm.^{2}

(iv) 227.87 kc/s; 75°C.

No.	P (cm.)	$p/_b$	$\lambda_{obs.}$ (cm.)
29	74	1.300_3	0.1642_9
30	74	1.300_7	0.1643_4
31	74	1.300_4	0.1643_0
32	74	1.299_6	0.1642_0
33	61	1.300_7	0.1643_6
34	61	1.300_2	0.1642_9
35	41	1.299_8	0.1642_6
36	41	1.300_3	0.1643_2

Theoretical $\lambda = 0.1640_3$ cm. Mean observed $\lambda = 0.1642_9$ cm.

$\frac{\Delta\lambda}{\lambda} = 0.0015_8$ $\lambda^2 = 0.0269$ cm.^{2}

Fig. 11 is the correction graph for the transverse wave effect at 228 kc/s.

(v) 695 kc/s; 25°C.

No.	P (cm.)	$p/_b$	$\lambda_{obs.}$ (cm.)
37	75	0.3946_3	0.4986_8
38	75	0.3948_9	0.4990_1
39	75	0.3951_2	0.4993_0
40	75	0.3950_1	0.4991_6
41	65	0.3952_7	0.4995_1

FIG. 12 — TRANSVERSE WAVE CORRECTION GRAPH — 695 kc/s

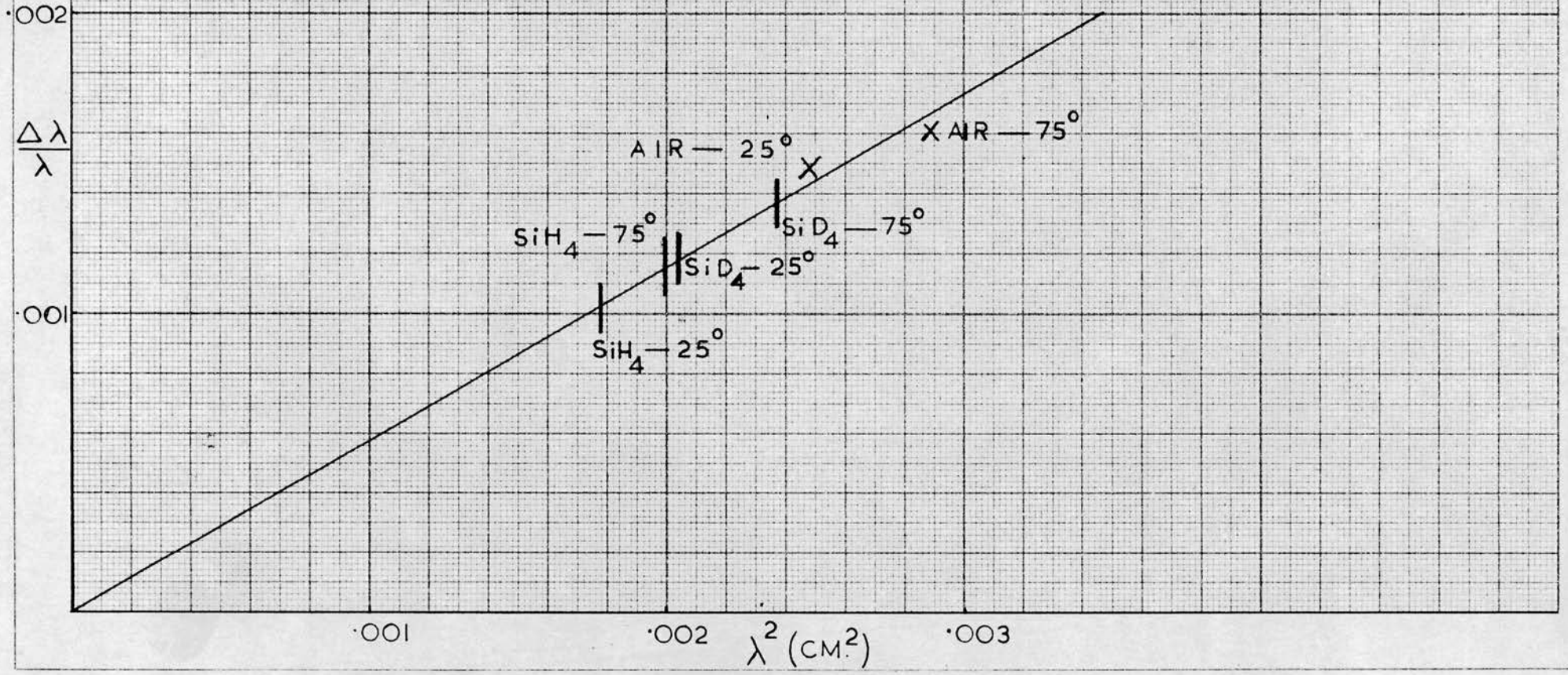

42	53	0.3944_2	0.4984_6
43	44	0.3946_6	0.4987_8
44	44	0.3947_8	0.4989_3

Theoretical $\lambda = 0.04982_3$ cm. Mean observed $\lambda = 0.4989_7$ cm.

$\frac{\Delta\lambda}{\lambda} = 0.0014_8$ $\lambda^2 = 0.00248$ cm.^{2}

(vi) 695 kc/s; 75°C.

No.	P (cm.)	p/b	λ_{obs} (cm.)
45	76	0.4266_7	0.05390_8
46	76	0.4272_2	0.05397_7
47	76	0.4269_4	0.05394_1
48	76	0.4265_9	0.05389_8
49	76	0.4269_1	0.05393_8

Theoretical $\lambda = 0.05384_5$ cm. Mean observed $\lambda = 0.05393_2$ cm.

$\frac{\Delta\lambda}{\lambda} = 0.0016_1$ $\lambda^2 = 0.00289$ cm.^{2}

Fig. 12 is the correction graph for the transverse wave effect at 695 kc/s.

2. Calibrations with Nitrogen

(i) 85.66 kc/s; 25°C.

No.	P (cm.)	p/b	$\lambda_{obs.}$ (cm.)
50	76	3.282_5	0.4147_9
51	76	3.284_6	0.4150_6
52	76	3.285_0	0.4151_1

Theoretical $\lambda = 0.4108_2$ cm. Mean observed $\lambda = 0.4149_9$ cm.

$\frac{\Delta\lambda}{\lambda} = 0.0102$ $\lambda^2 = 0.169$ cm.^{2}

Fig. 10 shows that this nitrogen calibration agrees well with the air calibrations.

3. Methane

(i) 85.66 kc/s; 25°C.

The observed wavelength of sound in methane at this frequency is between 0.526 and 0.529 cm. The mean transverse wave correction is thus 0.0172 (Fig. 10).

No.	P' (cm)	log f/P	p/b	$\lambda_{obs.}$ (cm)	λ_{corr} (cm)	V(m/s)	$V^2 \times 10^{-4}$
53	102.78	1.802	4.226_9	0.5347_6	0.5257_6	450.3_7	20.283
54	85.18	1.883	4.232_5	0.5353_8	0.5263_8	450.8_9	20.331
55	65.74	1.996	4.239_2	0.5361_5	0.5271_3	451.5_4	20.389
56	49.36	2.120	4.245_8	0.5369_0	0.5278_7	452.1_8	20.447
57	39.82	2.214	4.251_7	0.5376_0	0.5285_6	452.7_6	20.499
58	30.00	2.337	4.255_5	0.5380_3	0.5289_8	453.1_3	20.533
59	22.71	2.457	4.260_0	0.5385_8	0.5295_2	453.5_9	20.574
60	18.51	2.546	4.261_7	0.5387_7	0.5297_1	453.7_5	20.589
61	113.59	1.877	4.232_6	0.5355_2	0.5265_1	451.0_1	20.341
62	113.59	1.877	4.233_6	0.5356_5	0.5266_4	451.1_2	20.351
63	101.26	1.927	4.235_1	0.5357_8	0.5267_7	451.2_3	20.361
64	91.51	1.971	4.238_9	0.5362_3	0.5272_2	451.6_1	20.395
65	79.76	2.031	4.240_5	0.5363_7	0.5273_5	451.7_3	20.406
66	76.07	2.051	4.242_1	0.5365_5	0.5275_3	451.8_8	20.420
67	73.40	2.067	4.245_1	0.5369_2	0.5278_9	452.1_9	20.448
68	64.60	2.122	4.244_9	0.5368_5	0.5278_2	452.1_3	20.442
69	58.51	2.165	4.247_7	0.5371_7	0.5281_4	452.4_1	20.467
70	52.33	2.214	4.252_3	0.5377_4	0.5286_9	452.8_8	20.510
71	46.04	2.269	4.254_9	0.5380_3	0.5289_9	453.1_3	20.533
72	41.70	2.313	4.256_5	0.5382_1	0.5291_6	453.2_8	20.546
73	36.73	2.368	4.258_8	0.5384_8	0.5294_3	453.5_1	20.567
74	31.81	2.420	4.259_1	0.5385_0	0.5294_4	453.5_2	20.568
75	23.05	2.570	4.262_3	0.5388_6	0.5298_0	453.8_3	20.596
76	19.03	2.653	4.262_6	0.5388_5	0.5297_9	453.8_2	20.595

Results 53 - 60 were taken with the sample of methane obtained from Twentieth Century Electronics, Ltd., while results 61 -76 were taken with the methane prepared by the Grignard reaction. The two sets show good agreement.

FIG. 13

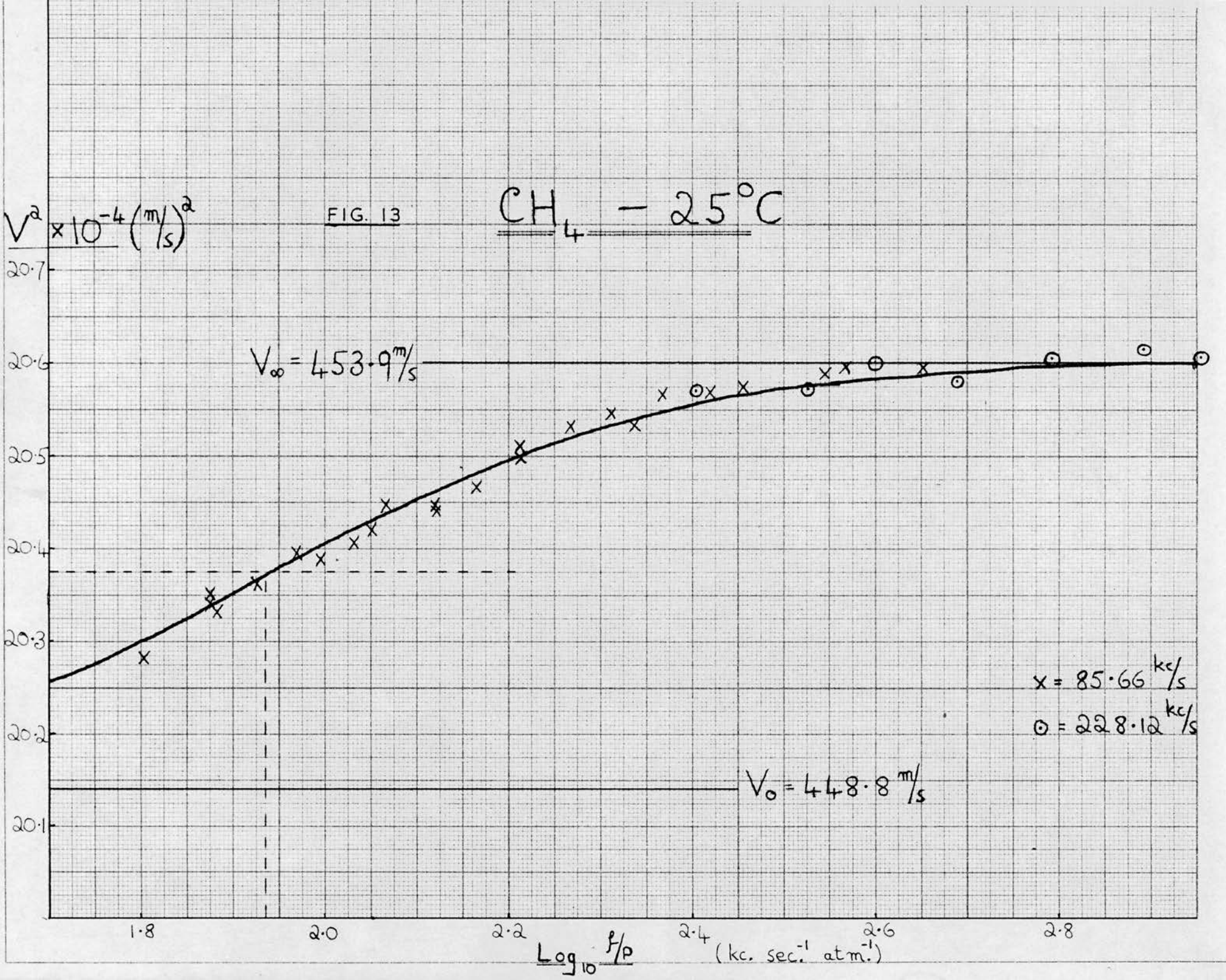
CH_4 – 25°C
$V^2 \times 10^{-4} (m/s)^2$
20·7
20·6
20·5
20·4
20·3
20·2
20·1
$V_\infty = 453.9 m/s$
$V_o = 448.8 m/s$
x = 85·66 kc/s
⊙ = 228·12 kc/s
1·8
2·0
2·2
2·4
2·6
2·8
$\text{Log}_{10} f/p$ (kc. sec.$^{-1}$ at m.$^{-1}$)

(ii) $228.12^{kc}/s$; $25^{\circ}C$.

The wavelength of sound at this frequency is 0.199 cm., and the transverse wave correction is 0.0025 (Fig. 11).

No.	P (cm)	log $^{f}/P$	$^{p}/b$	$\lambda_{obs.}$ (cm)	$\lambda_{corr.}$ (cm)	V($^{m}/s$	$V^2 \times 10^{-4}$
77	68.45	2.404	1.576_0	0.1993_2	0.1988_2	453.5_4	20.570
78	51.62	2.526	1.576_3	0.1993_3	0.1988_3	453.5_6	20.572
79	43.53	2.600	1.577_4	0.1994_6	0.1989_7	453.8_8	20.600
80	35.45	2.689	1.576_7	0.1993_6	0.1988_6	453.6_5	20.580
81	27.86	2.794	1.577_9	0.1994_9	0.1989_9	453.9_3	20.605
82	22.14	2.893	1.578_4	0.1995_4	0.1990_4	454.0_5	20.616
83	19.23	2.955	1.578_1	0.1995_0	0.1990_0	453.9_6	20.608

Results 77 - 83 were taken in the methane prepared by Grignard reaction.

The results are plotted in Fig. 13 with the theoretical curve calculated from equation 25. The lower end of the curve has not been defined as the pressures required are too high for the present apparatus. The point of inflection occurs at log $^{f}/P$ = 1.935, and the relaxation time is $2.0_3 \times 10^{-6}$ sec. at $25^{\circ}C$.

The values of the observed and corrected wavelengths are omitted from the remaining tables of results. They can readily be calculated from the tabulated values of $^{p}/b$ by the method given in the introduction to this chapter.

(iii) $\underline{85.75^{kc}/s;\ 75^{o}C}$

The wavelength of sound in methane at this frequency and temperature is between 0.563 and 0.567 cm. The mean transverse wave correction is thus 0.0195 (Fig. 10).

No.	P (cm.)	log $^{f}/_{p}$	$^{p}/_{b}$	V ($^{m}/_{s}$)	$V^2 \times 10^{-4}$
84	88.85	1.865	4.535_2	482.4_6	23.277
85	88.85	1.865	4.537_2	482.6_3	23.293
86	75.89	1.934	4.541_9	482.9_9	23.328
87	67.74	1.983	4.546_6	483.6_5	23.392
88	59.01	2.045	4.551_9	484.0_1	23.427
89	53.50	2.086	4.556_6	484.6_8	23.491
90	53.50	2.086	4.552_2	484.2_2	23.447
91	50.99	2.107	4.555_6	484.5_7	23.481
92	47.68	2.136	4.555_7	484.5_8	23.482
93	44.19	2.169	4.559_4	484.9_7	23.520
94	43.04	2.180	4.563_2	485.3_7	23.558
95	39.03	2.223	4.564_9	485.5_5	23.576
96	38.67	2.227	4.564_8	485.5_2	23.573
97	35.03	2.270	4.566_0	485.6_5	23.586
98	34.02	2.282	4.572_2	486.3_0	23.649
99	32.20	2.306	4.570_8	486.1_6	23.635
100	84.30	1.888	4.538_7	482.6_5	23.295
101	78.31	1.920	4.538_1	482.5_8	23.288
102	75.20	1.938	4.542_8	483.0_8	23.337
103	65.40	1.999	4.548_4	483.6_6	23.393
104	60.91	2.029	4.548_1	483.6_2	23.389

Results 84 - 99 were taken on redistilled cylinder methane and results 100 - 104 on methane prepared by the Grignard reaction.

FIG. 14 $CH_4 - 75°C$

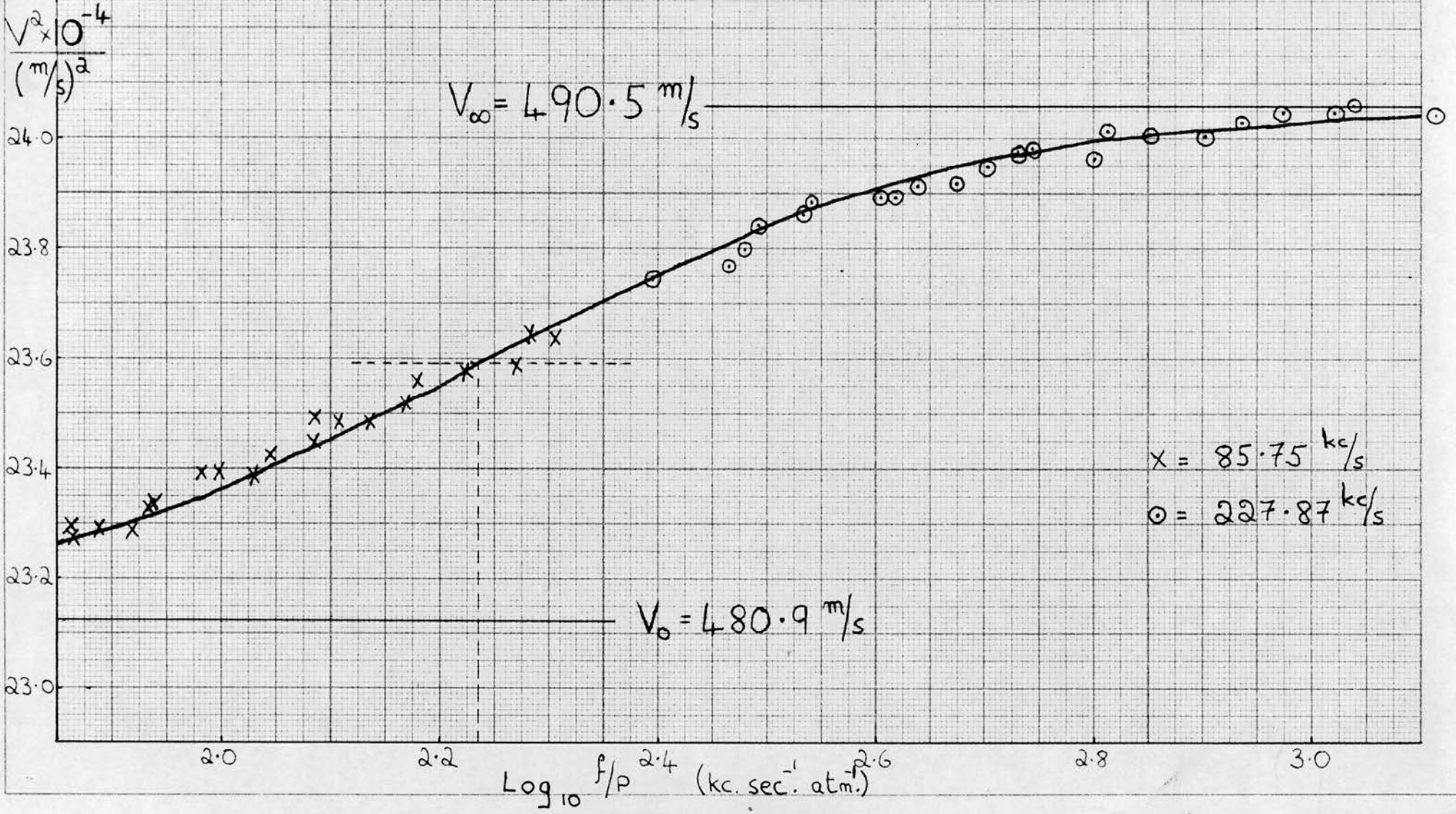

(iv) 227.87 kc/s; 75°C.

The wavelength of sound at this frequency is between 0.214 and 0.215 cm., and the transverse wave correction is 0.0030 (Fig. 11).

No.	P (cm.)	log f/p	p/b	V (m/s)	$V^2 \times 10^{-4}$
105	70.73	2.395	1.696_5	487.2_8	23.744
106	59.21	2.466	1.697_3	487.5_0	23.766
107	55.87	2.491	1.700_0	488.2_6	23.840
108	50.77	2.533	1.700_7	488.4_7	23.860
109	42.95	2.605	1.701_9	488.7_9	23.892
110	39.79	2.639	1.702_7	489.0_0	23.912
111	36.55	2.675	1.702_9	489.0_7	23.919
112	32.04	2.733	1.704_6	489.5_9	23.970
113	31.16	2.745	1.705_1	489.6_9	23.980
114	27.39	2.801	1.704_4	489.4_9	23.960
115	24.41	2.851	1.706_1	489.9_6	24.006
116	21.69	2.902	1.706_0	489.9_3	24.003
117	20.03	2.937	1.706_9	490.1_9	24.029
118	18.38	2.974	1.707_6	490.4_0	24.049
119	16.47	3.022	1.707_6	490.36	24.045
120	15.85	3.038	1.708_1	490.5_7	24.060
121	12.91	3.127	1.707_4	490.3_1	24.040
122	57.30	2.480	1.698_4	487.8_2	23.797
123	48.95	2.541	1.701_5	488.6_9	23.881
124	41.74	2.618	1.701_9	488.7_8	23.891
125	34.30	2.703	1.703_9	489.3_6	23.947
126	26.57	2.814	1.706_2	490.0_1	24.011

Results 105 - 121 were taken on redistilled cylinder methane, and results 122 - 126 on methane prepared by the Grignard reaction.

The results are shown in Fig. 14 with the theoretical curve. The lower end of the curve is again not defined, but the point of inflection occurs at log $^{f}/P$ = 2.235, and the relaxation time is 1.10 x 10^{-6} sec. at 75°C.

4. Tetradeuteromethane

(i) 85.66 $^{kc}/s$; 25°C.

The wavelength of sound in tetradeuteromethane is between 0.467 and 0.474 cm. at this frequency. The mean transverse wave correction is 0.0137. (Fig. 10).

No.	P (cm.)	log $^{f}/p$	p/b	V ($^{m}/s$)	V^2 x 10^{-4}
127	122.16	1.727	3.741_2	400.0_2	16.002
128	111.74	1.766	3.744_5	400.3_3	16.026
129	103.42	1.799	3.751_0	401.0_1	16.081
130	94.96	1.836	3.752_9	401.1_8	16.095
131	88.57	1.867	3.759_3	401.8_4	16.148
132	88.57	1.867	3.758_9	401.8_1	16.145
133	79.33	1.914	3.762_6	402.1_7	16.174
134	70.19	1.967	3.767_3	402.7_2	16.218
135	65.00	2.008	3.774_1	403.4_2	16.275
136	57.84	2.056	3.774_9	403.4_8	16.280
137	51.39	2.103	3.778_3	403.8_1	16.306
138	45.79	2.153	3.780_1	404.0_0	16.322
139	39.72	2.215	3.786_4	404.6_5	16.374
140	33.94	2.283	3.788_8	404.8_8	16.393
141	32.22	2.306	3.792_9	405.2_8	16.422
142	28.53	2.358	3.793_6	405.3_4	16.427
143	26.10	2.397	3.798_1	405.7_0	16.461
144	22.82	2.455	3.797_8	405.7_3	16.461
145	19.75	2.518	3.798_2	405.7_6	16.464
146	16.77	2.589	3.800_3	405.9_7	16.481

FIG. 15 $CD_4 - 25°C$

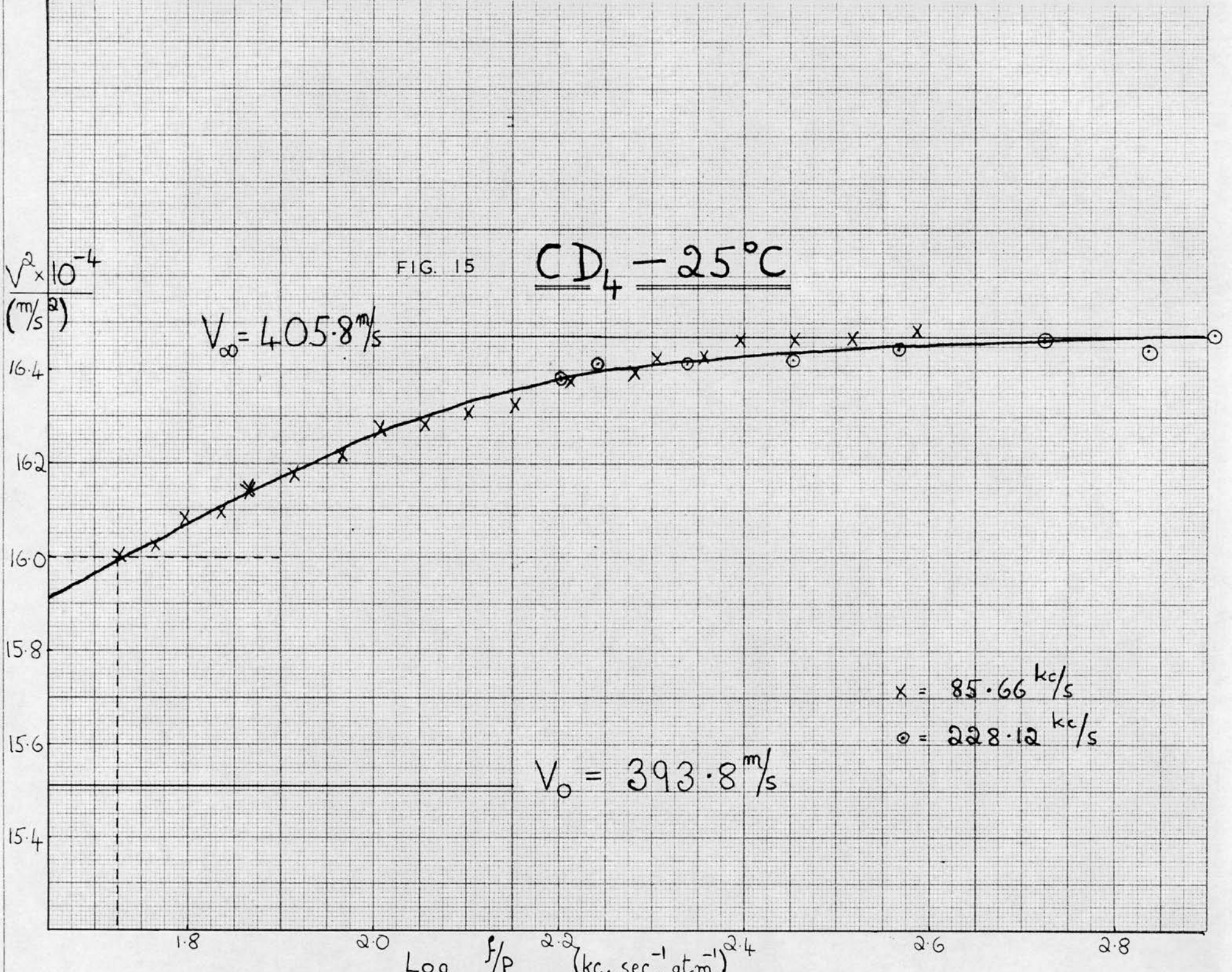

(ii) 228.12 kc/s; 25°C.

The wavelength of sound at this frequency and temperature is 0.178 cm, and the transverse wave correction is 0.0021 (Fig. 11).

No.	P (cm.)	log f/p	p/b	V (m/s)	$V^2 \times 10^{-4}$
147	109.12	2.201	1.405_2	404.7_4	16.381
148	99.25	2.242	1.406_6	405.1_0	16.411
149	79.54	2.339	1.406_8	405.1_0	16.411
150	61.04	2.453	1.407_4	405.2_2	16.420
151	46.98	2.567	1.408_6	405.5_0	16.443
152	32.69	2.725	1.409_6	405.7_6	16.464
153	25.11	2.839	1.408_7	405.4_6	16.440
154	21.17	2.913	1.410_2	405.9_0	16.475
155	17.22	2.003	1.409_7	405.7_3	16.462

The dispersion curve is shown in Fig. 15. The point of inflection occurs at log f/p = 1.725, and the relaxation time is $3.9_0 \times 10^{-6}$ sec. at 25°C.

(iii) 85.75 kc/s; 75°C.

Here λ is between 0.496 and 0.510 cm., and $\frac{\Delta\lambda}{\lambda} = 0.0156$.

No.	P (cm.)	log f/p	p/b	V (m/s)	$V^2 \times 10^{-4}$
156	117.09	1.745	3.984_6	425.4_1	18.097
157	117.09	1.745	3.982_5	425.1_8	18.078
158	106.90	1.785	3.994_1	426.4_1	18.183
159	96.04	1.832	3.995_9	426.5_9	18.198
160	88.34	1.868	4.007_7	427.8_3	18.304
161	80.15	1.910	4.011_2	428.1_9	18.335
162	74.48	1.942	4.020_5	429.2_2	18.423
163	68.39	1.979	4.024_7	429.6_2	18.457
164	63.55	2.011	4.032_2	430.4_2	18.526
165	58.72	2.045	4.036_6	430.8_8	18.566
166	55.76	2.068	4.046_4	431.9_2	18.655
167	48.10	2.132	4.059_2	433.2_7	18.772
168	42.77	2.183	4.060_4	433.4_0	18.784
169	41.00	2.201	4.067_4	434.1_4	18.848
170	36.35	2.254	4.075_3	434.9_8	18.921
171	33.08	2.295	4.078_6	435.2_8	18.947
172	31.00	2.323	4.083_1	435.7_9	18.991
173	28.36	2.361	4.084_7	435.9_3	19.003
174	23.74	2.439	4.091_4	436.6_8	19.069
175	21.51	2.481	4.092_5	436.7_9	19.079
176	20.32	2.506	4.095_3	437.0_9	19.105
177	18.48	2.547	4.101_1	437.7_2	19.160
178	14.26	2.660	4.102_4	437.8_4	19.170

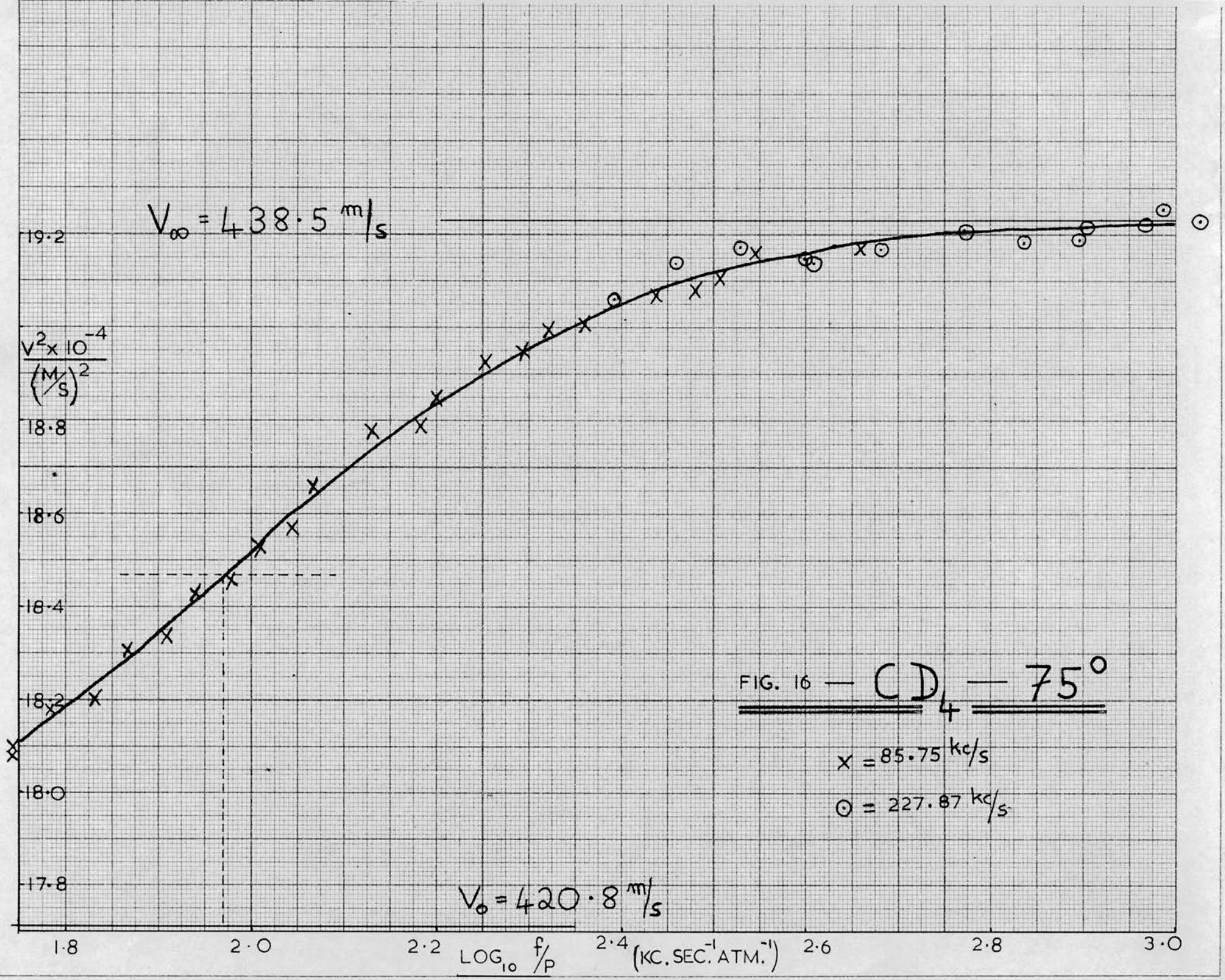
$V_\infty = 438.5$ m/s
$V_0 = 420.8$ m/s
$\frac{V^2 \times 10^{-4}}{(M/S)^2}$
19·2
18·8
18·6
18·4
18·2
18·0
17·8
1·8
2·0
2·2
2·4
2·6
2·8
3·0
$\log_{10} f/P$ (KC. SEC.$^{-1}$ ATM.$^{-1}$)
FIG. 16 — CD_4 — 75°
× = 85.75 kc/s
⊙ = 227.87 kc/s

(iv) 227.87 kc/s; 75°C

The wavelength of sound is 0.192 cm., and the transverse wave correction is 0.0024 (Fig. 11).

No.	P (cm.)	log f/p	p/b	V (m/s)	$V^2 \times 10^{-4}$
179	70.07	2.393	1.519_1	436.5_8	19.060
180	60.30	2.458	1.522_2	437.4_8	19.139
181	51.20	2.529	1.523_6	437.8_6	19.172
182	43.71	2.598	1.522_7	437.5_9	19.149
183	42.70	2.608	1.522_3	437.4_6	19.137
184	36.09	2.681	1.523_1	437.7_0	19.158
185	29.37	2.771	1.525_1	438.2_7	19.208
186	25.26	2.836	1.524_1	437.9_6	19.181
187	21.95	2.897	1.524_4	438.0_4	19.188
188	21.57	2.905	1.525_4	438.3_4	19.214
189	18.60	2.969	1.525_7	438.4_1	19.220
190	17.89	2.986	1.527_1	438.8_1	19.255
191	15.86	3.038	1.526_1	438.5_1	19.229

The dispersion curve is shown in Fig. 16. The point of inflection occurs at log f/p = 1.970 and the relaxation time is $2.5_0 \times 10^{-6}$ sec. at 75°C.

5. Silane

(i) 85.66 kc/s; 25°C.

The wavelength of sound in silane at this frequency is 0.361 cm., and the transverse wave correction factor is 0.0081. (Fig. 10).

No.	P (cm.)	log f/p	p/b	V (m/s)	$V^2 \times 10^{-4}$
192	70.15	1.968	2.867_7	309.1_6	9.558
193	60.81	2.030	2.870_4	309.0_2	9.549
194	59.46	2.040	2.870_2	309.0_4	9.551
195	49.42	2.120	2.869_1	308.7_4	9.532
196	47.64	2.136	2.872_7	309.1_1	9.555
197	41.06	2.200	2.872_5	309.0_1	9.549
198	40.01	2.216	2.873_6	309.1_2	9.556
199	39.20	2.221	2.873_0	309.0_4	9.551
200	34.30	2.279	2.875_0	309.2_1	9.561
201	31.95	2.309	2.873_5	309.0_1	9.549
202	25.38	2.408	2.876_4	309.2_4	9.563

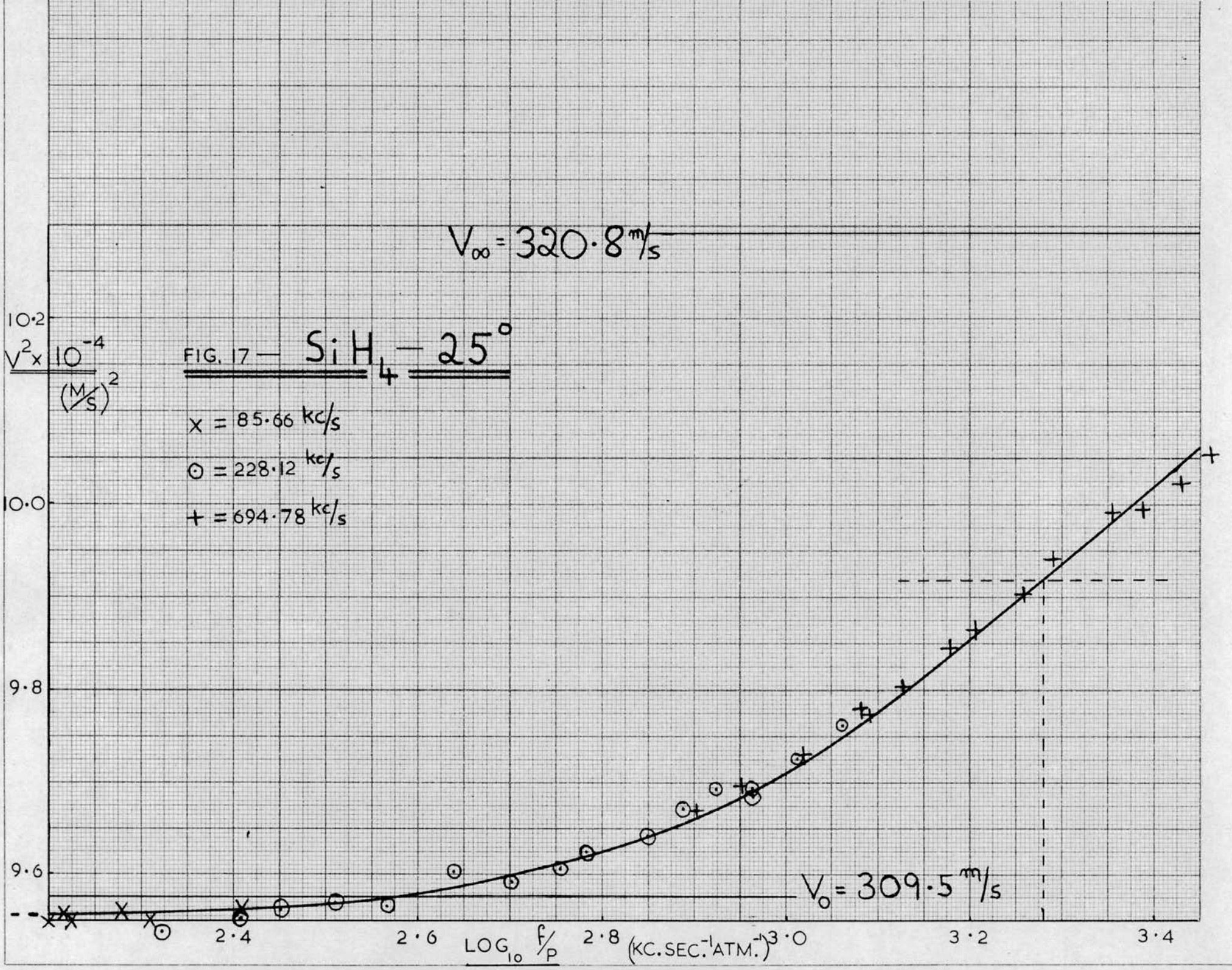
$V_\infty = 320.8$ m/s
10·2
$V^2 \times 10^{-4}$ / $(M/S)^2$
FIG. 17 — SiH_4 — 25°
X = 85.66 kc/s
⊙ = 228.12 kc/s
+ = 694.78 kc/s
10·0
9·8
9·6
$V_0 = 309.5$ m/s
2·4
2·6
2·8
3·0
3·2
3·4
$LOG_{10}\ f/p$ (KC. SEC.$^{-1}$ ATM.$^{-1}$)

(ii) 228.12 kc/s; 25°C

The wavelength of sound at this frequency is 0.136 cm., and the transverse wave correction factor is 0.0012 (Fig. 11).

No.	P (cm.)	log f/p	p/b	V (m/s)	$V^2 \times 10^{-4}$
203	73.60	2.372	1.069_2	308.8_0	9.536
204	67.96	2.407	1.070_4	309.0_8	9.553
205	61.58	2.450	1.071_2	309.2_5	9.564
206	53.67	2.510	1.071_9	309.3_6	9.570
207	47.12	2.566	1.071_9	309.2_7	9.565
208	40.03	2.637	1.074_3	309.8_8	9.603
209	34.57	2.701	1.074_0	309.7_1	9.592
210	30.49	2.755	1.074_9	309.9_4	9.606
211	28.59	2.783	1.076_1	310.2_4	9.625
212	24.57	2.849	1.077_1	310.5_1	9.642
213	22.53	2.887	1.078_9	311.0_0	9.672
214	20.69	2.924	1.080_3	311.3_5	9.694
215	18.87	2.964	1.080_3	311.3_5	9.694
216	18.87	2.964	1.079_9	311.2_4	9.687
217	16.90	3.012	1.082_2	311.8_7	9.727
218	15.00	3.063	1.084_2	312.42	9.761

(iii) 694.78 kc/s; 25°C.

The wavelength of sound is between 0.0448 and 0.0456 cm., and the mean transverse wave correction factor is 0.0011_6. (Fig. 12).

No.	P (cm.)	log f/p	p/b	V (m/s)	$V^2 \times 10^{-4}$
219	66.25	2.902	0.35357	310.9_5	9.669
220	58.62	2.955	0.3541_8	311.3_9	9.696
221	50.71	3.018	0.3549_0	311.9_3	9.730
222	43.58	3.083	0.3559_3	312.7_4	9.781
223	42.85	3.091	0.3557_5	312.5_9	9.771
224	39.30	3.128	0.3564_2	313.1_2	9.804
225	34.97	3.179	0.3572_3	313.7_9	9.846
226	32.78	3.207	0.3576_1	314.0_9	9.865
227	29.09	3.259	0.3583_3	314.6_7	9.902
228	26.99	3.292	0.3590_9	315.3_2	9.943
229	23.32	3.355	0.3600_1	316.0_8	9.991
230	21.53	3.389	0.3601_2	316.1_5	9.995
231	19.67	3.429	0.3606_1	316.5_7	10.022
232	17.92	3.469	0.3611_9	317.0_5	10.052

These results are plotted in Fig. 17 with the theoretical curve calculated from eqn. 25. The observed and calculated values of V_o^2 differ by about

FIG. 18 — SiH_4 — 75°

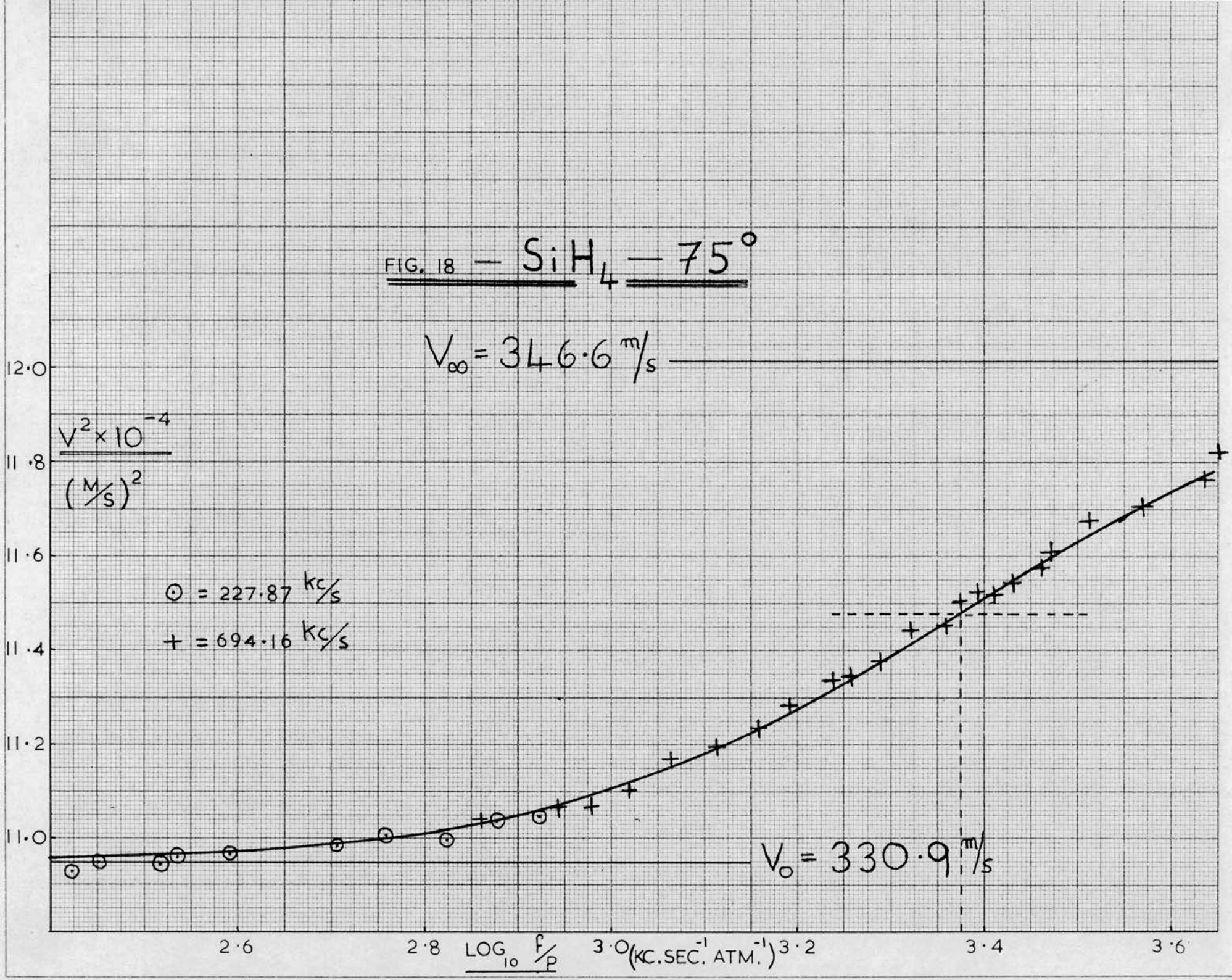

1 in 600, but this is probably due to the small uncertainty in the viral correction. When an allowance is made for this discrepancy the point of inflection occurs at log $^{f}/p = 3.280$ and the relaxation time is 1.15×10^{-7} sec. at 25°C.

(iv) 227.87 $^{kc}/s$; 75°C.

At this temperature the wavelength of sound is 0.145 cm., and the transverse wave correction factor is 0.0013_8. (Fig. 11).

No.	P (cm.)	log $^{f}/p$	p/b	V ($^{m}/s$)	$V^2 \times 10^{-4}$
233	65.45	2.423	1.147_7	330.5_9	10.929
234	61.29	2.451	1.148_9	330.9_1	10.950
235	52.83	2.516	1.148_9	330.8_5	10.946
236	50.48	2.535	1.149_7	331.0_4	10.959
237	44.39	2.591	1.150_1	331.1_1	10.963
238	34.06	2.706	1.151_3	331.3_7	10.981
239	30.22	2.758	1.152_6	331.7_6	11.006
240	25.96	2.824	1.152_3	331.6_8	10.998
241	23.01	2.877	1.154_4	332.2_2	11.037
242	20.72	2.922	1.155_1	332.3_8	11.048

(v) 694.16 $^{kc}/s$; 75°C.

The wavelength of sound is between 0.0479 and 0.0494 cm., and the mean transverse wave correction factor is 0.0013_3. (Fig. 12).

No.	P (cm.)	log $^{f}/p$	p/b	V ($^{m}/s$)	$V^2 \times 10^{-4}$
243	72.62	2.861	0.3785_9	332.2_7	11.040
244	60.05	2.944	0.3790_6	332.5_9	11.062
245	55.52	2.978	0.3791_5	332.6_8	11.068
246	50.45	3.019	0.3798_1	333.2_2	11.104
247	45.49	3.064	0.3809_7	334.2_0	11.169
248	40.62	3.114	0.3814_8	334.6_1	11.196
249	36.69	3.158	0.3821_4	335.1_7	11.234
250	33.85	3.193	0.3829_7	335.8_7	11.281
251	30.33	3.240	0.3839_6	336.7_1	11.337
252	29.10	3.258	0.3840_9	336.8_2	11.345
253	27.11	3.290	0.3846_9	337.3_2	11.378
254	25.06	3.323	0.3857_5	338.2_4	11.441
255	23.13	3.358	0.3859_5	338.4_1	11.452
256	22.26	3.375	0.3868_6	339.1_5	11.502
257	21.29	3.394	0.3871_7	339.4_6	11.523
258	20.48	3.411	0.3871_3	339.3_7	11.517
259	19.57	3.431	0.3875_3	339.7_7	11.544
260	18.15	3.463	0.3881_1	340.2_2	11.575
261	17.80	3.472	0.3886_7	340.7_0	11.608
262	16.10	3.515	0.3897_3	341.6_6	11.673
263	14.19	3.570	0.3903_6	342.1_6	11.707
264	12.21	3.636	0.3913_1	342.9_8	11.764
265	11.77	3.651	0.3922_1	343.8_1	11.821

The dispersion curve is shown in Fig. 18. The virial correction is smaller at the higher temperature, and observed and calculated values of V_o agree more closely. The point of inflection occurs at log $^f/_p$ = 3.375 and the relaxation time is 1.04×10^{-7} sec. at 75°C.

6. Tetradeuterosilane

(i) 85.66 kc/s; 25°C.

The wavelength of sound in tetradeutersilane at this frequency is 0.333 cm., and the transverse wave correction factor is 0.0071. (Fig. 10).

No.	P (cm.)	log $^f/_p$	$^p/_b$	V ($^m/_s$)	$V^2 \times 10^{-4}$
266	76.80	1.928	2.644_7	285.1_9	8.133
267	76.80	1.928	2.644_8	285.2_0	8.134
268	69.37	1.973	2.647_1	285.3_6	8.143
269	61.58	2.024	2.648_2	285.3_9	8.145
270	53.48	2.086	2.649_2	285.4_4	8.148
271	45.88	2.152	2.648_8	285.2_9	8.139
272	38.01	2.234	2.647_7	285.0_7	8.126
273	32.33	2.304	2.648_8	285.1_3	8.130
274	29.70	2.341	2.648_9	285.1_2	8.129
275	26.88	2.384	2.649_7	285.1_7	8.132
276	25.00	2.416	2.653_5	285.5_6	8.154
277	23.15	2.449	2.655_9	285.8_0	8.168
278	21.02	2.491	2.656_7	285.8_5	8.171
279	18.87	2.538	2.660_1	286.2_0	8.191
280	17.08	2.581	2.664_0	286.6_0	8.214

(ii) 228.12 kc/s; 25°C.

The wavelength of sound at this frequency is between 0.125 and 0.127 cm., and the transverse wave correction factor is 0.0010_4 (Fig. 11).

No.	P (cm.)	log $^f/_p$	$^p/_b$	V ($^m/_s$)	$V^2 \times 10^{-4}$
281	77.12	2.352	0.986_7^6	285.0_9	8.128
282	54.81	2.500	0.990_4^3	285.8_7	8.172
283	46.84	2.568	0.992_6^3	286.3_7	8.201
284	39.61	2.642	0.993_2^9	286.7_4	8.222
285	34.00	2.708	0.995_2^1	287.0_2	8.238
286	29.91	2.763	0.997_1^6	287.6_9	8.277
287	27.80	2.795	0.998_0^6	287.8_0	8.283
288	25.75	2.828	1.001_2	288.6_8	8.334
289	23.88	2.861	1.002_4	289.0_1	8.353
290	22.93	2.879	1.003_8	289.4_0	8.375

FIG. 19 — SiD_4 — 25°

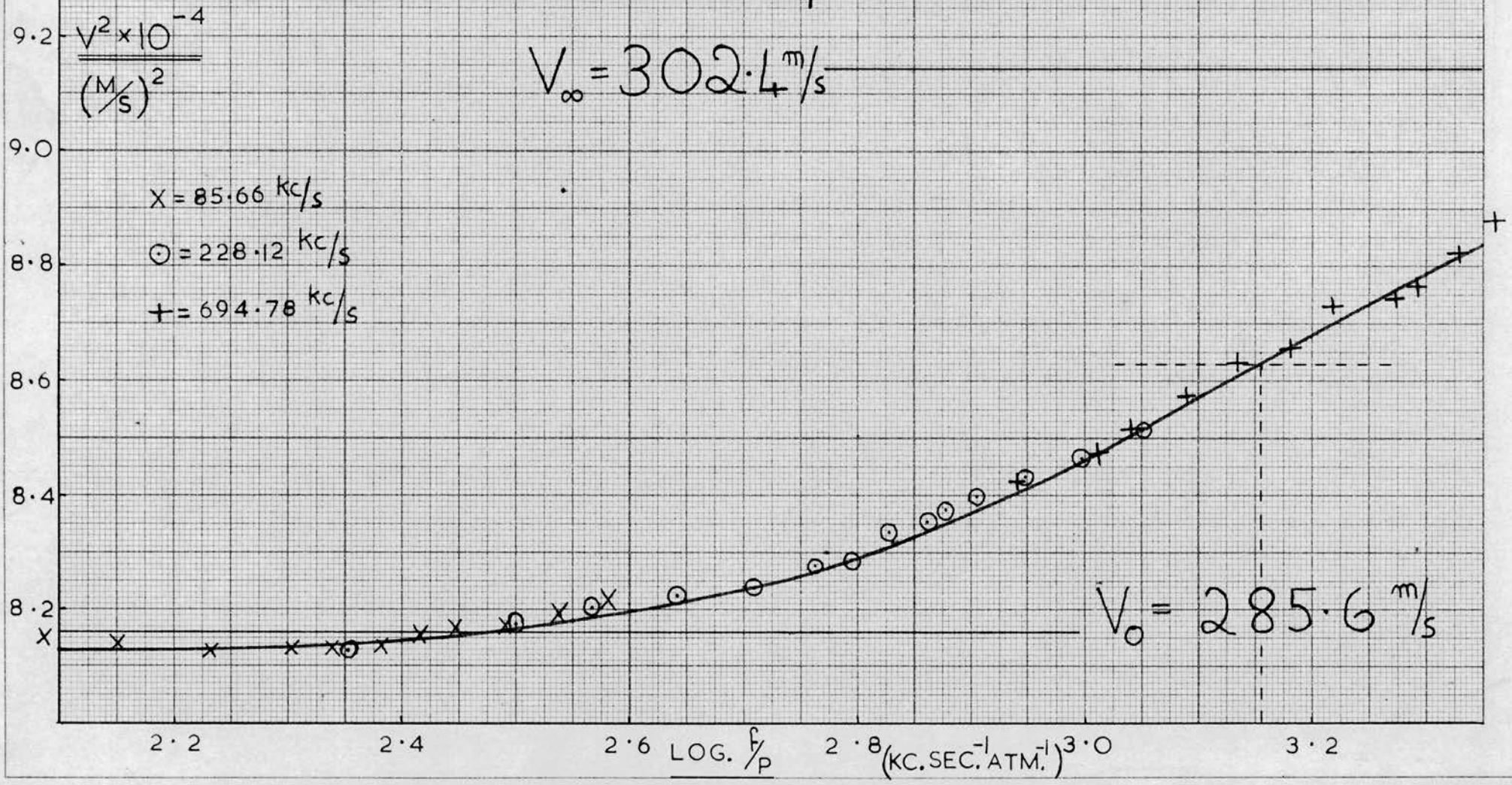

291	21.61	2.905	1.005_2	289.7_9	8.398
292	19.50	2.949	1.007_3	290.3_7	8.431
293	17.45	2.997	1.009_1	290.8_8	8.461
294	15.42	3.051	1.012_5	291.8_2	8.516

(iii) 694.78 kc/s; 25°C

The wavelength of sound is between 0.0418 and 0.0428 cm., and the transverse wave correction factor is 0.0010_2. (Fig. 12).

No.	P (cm.)	log $^f/_p$	$^p/_b$	V($^m/_s$)	$V^2 \times 10^{-4}$
295	60.15	2.943	0.3301_3	290.3_0	8.427
296	60.15	2.943	0.3300_1	290.2_0	8.422
297	51.39	3.012	0.3311_6	291.1_1	8.475
298	47.95	3.042	0.3320_4	291.8_5	8.518
299	42.80	3.090	0.3331_9	292.8_0	8.573
300	38.69	3.135	0.3343_8	293.7_9	8.631
301	34.80	3.181	0.3349_0	294.2_0	8.655
302	31.89	3.219	0.3364_0	295.4_9	8.731
303	28.17	3.273	0.3367_0	295.7_1	8.744
304	26.88	3.293	0.3371_0	296.0_5	8.765
305	24.78	3.329	0.3382_1	297.0_0	8.821
306	22.78	3.365	0.3393_5	297.9_8	8.879
307	20.77	3.405	0.3398_8	298.4_2	8.905
308	18.76	3.450	0.3407_0	299.1_2	8.947

Fig. 19 shows the dispersion curve. Despite the difference of only 14 $cm.^{-1}$ between ν_2 and ν_4 of tetradeuterosilane, there is no evidence for double dispersion. As in the case of silane at 25°C, the calculated and experimental values of V_o differ by about 1 in 500 due to uncertainties in the virial correction. When an allowance is made for this discrepancy, the point of inflection occurs at log $^f/_p$ = 3.155, and the relaxation time is 1.96×10^{-7} sec. at 25°C.

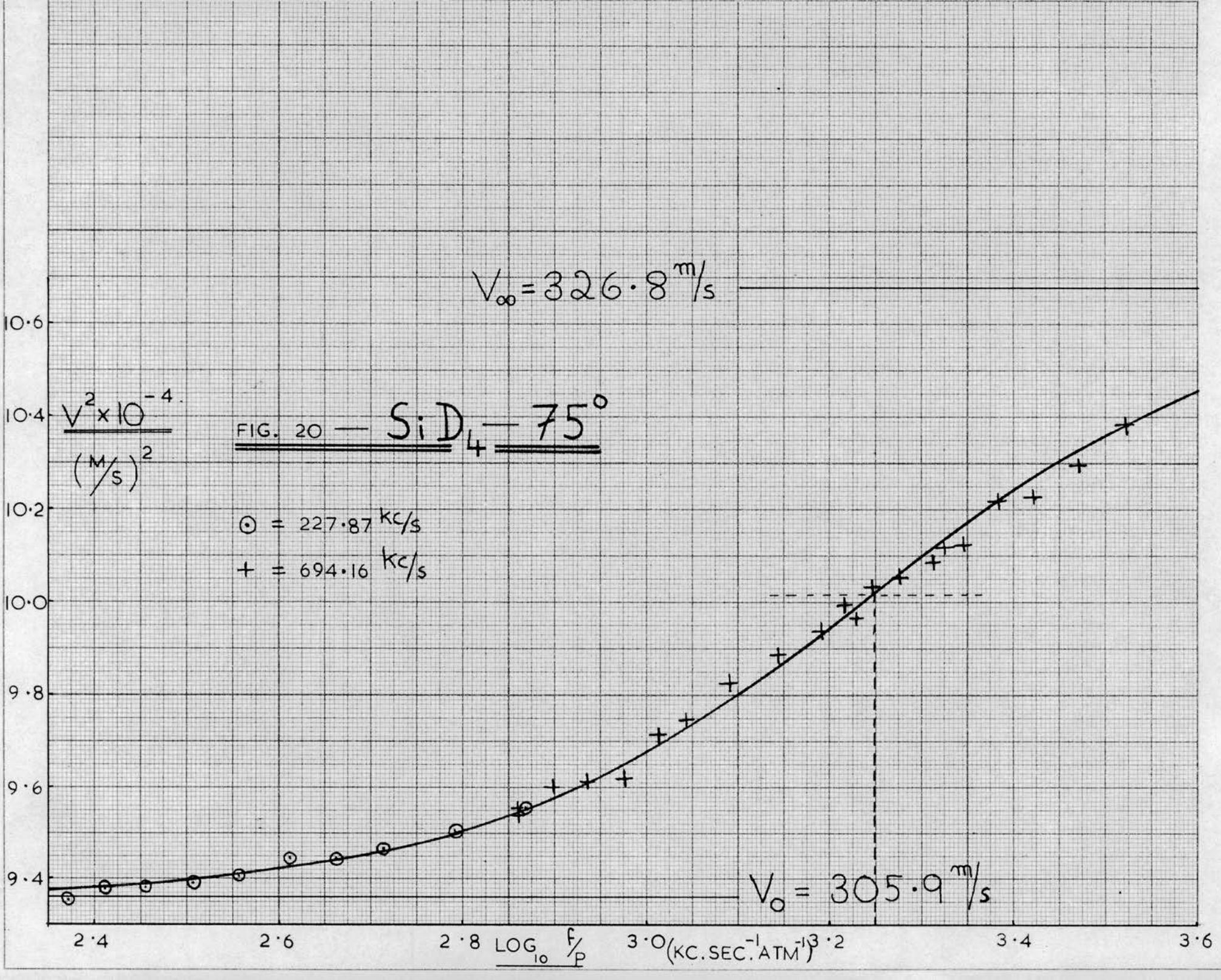
$V_\infty = 326.8$ m/s
$\frac{V^2 \times 10^{-4}}{(M/S)^2}$
FIG. 20 — SiD_4 — 75°
⊙ = 227.87 kc/s
+ = 694.16 kc/s
$V_o = 305.9$ m/s
10·6
10·4
10·2
10·0
9·8
9·6
9·4
2·4
2·6
2·8
3·0
3·2
3·4
3·6
$\log_{10} f/p$ (KC.SEC.$^{-1}$ATM.$^{-1}$)

(iv) 227.87 kc/s; 75°C.

The wavelength of sound at this frequency and temperature is 0.135 cm., and the transverse wave correction factor is 0.0011_8. (Fig. 11).

No.	P (cm.)	$\log f/p$	p/b	V (m/s)	$V^2 \times 10^{-4}$
309	73.73	2.371	1.061_4	305.8_5	9.354
310	67.22	2.411	1.062_9	306.2_3	9.378
311	60.74	2.455	1.063_2	306.2_7	9.380
312	53.83	2.507	1.063_9	306.4_4	9.390
313	48.10	2.556	1.064_9	306.6_7	9.405
314	42.21	2.613	1.067_2	307.3_1	9.444
315	37.63	2.663	1.067_5	307.3_5	9.446
316	33.49	2.714	1.068_7	307.6_8	9.467
317	27.96	2.792	1.070_9	308.2_8	9.504
318	23.50	2.868	1.074_0	309.1_3	9.556

(v) 694.16 kc/s; 75°C.

The wavelength of sound is between 0.0445 and 0.0462 cm., and the mean transverse wave correction factor is 0.0011_5 (Fig. 12).

No.	P (cm.)	$\log f/p$	p/b	V (m/s)	$V^2 \times 10^{-4}$
319	72.59	2.861	0.3518_4	308.8_5	9.539
320	72.59	2.861	0.3521_4	309.1_1	9.555
321	70.45	2.874	0.3523_2	309.2_5	9.564
322	66.72	2.898	0.3530_1	309.8_4	9.600
323	61.09	2.936	0.3532_8	310.0_3	9.612
324	55.77	2.976	0.3534_6	310.1_5	9.619
325	51.16	3.013	0.3551_9	311.6_4	9.712
326	47.55	3.045	0.3558_5	312.2_8	9.747
327	42.53	3.093	0.3573_3	313.4_5	9.825
328	37.80	3.145	0.3584_4	314.4_2	9.886
329	34.00	3.191	0.3594_6	315.2_6	9.939
330	32.01	3.217	0.3604_8	316.1_5	9.995
331	31.05	3.230	0.3599_4	315.6_7	9.965
332	29.83	3.248	0.3611_6	316.7_3	10.032
333	27.94	3.276	0.3615_4	317.0_5	10.052
334	25.68	3.313	0.3621_5	317.5_7	10.085
335	24.98	3.325	0.3627_6	318.1_0	10.119
336	23.71	3.347	0.3635_2	318.7_6	10.161
337	21.80	3.384	0.3645_5	319.6_5	10.218
338	19.90	3.423	0.3647_3	319.7_9	10.227
339	17.85	3.471	0.3660_0	320.8_9	10.297
340	15.87	3.522	0.3675_6	322.2_5	10.385

The dispersion curve is shown in Fig. 20. The point of inflection occurs at $\log f/p = 3.247$ and the relaxation time is 1.78×10^{-7} sec. at 75°C.

7. Summary of Results

Table 1 summarises the values obtained for the relaxation times (in microseconds).

TABLE 1

	25°C	75°C
CH_4	2.0_3 (± 0.2)	1.1_0 (± 0.08)
CD_4	3.9_0 (± 0.2)	2.5_0 (± 0.15)
SiH_4	0.115 (± 0.006)	0.104 (± 0.006)
SiD_4	0.196 (± 0.011)	0.178 (± 0.011)

The errors have been estimated from the scatter of the points on the dispersion curves.

CHAPTER 7

DISCUSSION

(i) Relaxation time of methane.

Four sets of measurements of the relaxation time of methane have been reported previously, and these are given in Table II, along with the present results for comparison.

TABLE II - RELAXATION TIME OF METHANE

T °C	$\tau \times 10^6$ (sec.)	Reference
16	0.48	Griffith[20]
25	1.86	Edmonds and Lamb[21]
25	2.03	Matheson
30	1.68	Cottrell and Martin[22]
60	1.72	"
75	1.10	Matheson
109	0.84	Eucken and Aybar[23]
200	0.67	"
204	0.65	"
301	0.58	"
322	0.51	"
353	0.49	"

It is unlikely that any of these values are more accurate than $\pm 10\%$. Edmonds and Lamb measured absorption by a reverberation technique, while Cottrell and Martin, and Eucken and Aybar measured velocity dispersion. All these investigators used natural gas purified by conventional distillation. Griffith used the impact tube method with methane containing 1% of ethane,

and his result is low. The author has found that conventional distillation of natural gas will not reduce the percentage of air in methane below about 0.5 to 1%, or the percentage of ethane below 0.1%. Because of the considerable effect of impurities it is probable that some of these results are slightly low.

The measurements of Cottrell and Martin, made in the present interferometer, show a negative temperature dependence. There are two opposing factors which may explain their results. They did not purify their methane exhaustively, or specifically analyse for higher hydrocarbons, and they should thus have obtained a low relaxation time at both temperatures. On the other hand they did not fit their results to a theoretically calculated dispersion curve nor did they correct for transverse waves. This means that their observed velocities were too high, and that the upper limit of the dispersion curve was not reached. The observed relaxation times should thus be too long. The latter effect is greater at 60°C than at 30°C due to the larger transverse wave correction factor there, and this may explain their negative temperature dependence. These effects are particularly pronounced in methane where the dispersion region is narrow and the transverse wave correction large. Accordingly no relaxation times obtained from velocity dispersion can be considered reliable unless the results have been fitted to a theoretical curve, one end of which is adequately defined experimentally.

(ii) Temperature dependence of the relaxation times

As expected, the relaxation times of these molecules are shorter at 75°C than at 25°C. In the case of the silanes where the relaxation times are comparatively short, the differences in the relaxation times at

the two temperatures are small and of the same order as the experimental error. The methanes have longer relaxation times and a much greater temperature dependence. This result is in agreement with the well-established tendency of molecules with long relaxation times to show a steeper temperature dependence of relaxation time than that shown by molecules with short relaxation times.

(iii) Comparison of the relaxation times of isotopic molecules.

At both temperatures the relaxation times of the deuterated molecules are considerably longer than those of their hydrogenated counterparts:

$$\frac{\tau_{CD_4}}{\tau_{CH_4}} = 1.9_2 \quad \text{and} \quad \frac{\tau_{SiD_4}}{\tau_{SiH_4}} = 1.7_0 \quad \text{at } 25^\circ C$$

$$\text{and} \quad \frac{\tau_{CD_4}}{\tau_{CH_4}} = 2.2_7 \quad \text{and} \quad \frac{\tau_{SiD_4}}{\tau_{SiH_4}} = 1.7_1 \quad \text{at } 75^\circ C$$

The relaxation times of two other deuterated compounds have been reported. Lambert and Salter[24] gave τ for trideuteromethyl bromide at 25°C as 14.2 x 10^{-8} sec., while reported values of τ for methyl bromide are 7.2 x 10^{-8} sec. at 18°C[25] and 7.5 x 10^{-8} sec. at 27°C[26], giving $\frac{\tau_{CD_3Br}}{\tau_{CH_3Br}} = 1.9$ approximately. Hudson, McCoubrey and Ubbelohde[27] predict that the relaxation time of ethylene should be from 3.5 to 8 times as long as that of tetradeuteroethylene. Experimentally they find that, while $\tau_{C_2H_4}$ is longer than $\tau_{C_2D_4}$, the ratio $\frac{\tau_{C_2H_4}}{\tau_{C_2D_4}}$ is only 1.8.

The usual theories of translational-vibrational energy transfer predict that the relaxation times of the deuterated compounds should be shorter than those of the hydrogenated ones. During the time in which two gas molecules are in collision, say 3×10^{-13} sec., a typical molecular frequency of 1000 cm.$^{-1}$ executes about 10 vibrations. But for energy transfer to take place, the time of an encounter and the period of the molecular vibration must be similar. Thus the greater is the translational velocity of a molecule, the shorter is the time of an encounter, and the greater is the probability of energy transfer in a collision. Likewise the lower is the frequency of the molecular vibration, the greater is the probability of energy transfer. Thus the slightly greater mass of a deuterated molecule leads to a slower average relative translational velocity and to a relaxation time slightly longer than that of the hydrogenated molecule. This effect is outweighed, however, by the lower fundamental vibration frequencies of the deuterated molecule which leads to a greater probability of energy transfer and hence to a shorter relaxation time. This simple picture of energy transfer thus cannot account for the longer relaxation times of the deuterated molecules.

A related phenomenon occurs in the Lambert-Salter plot of the logarithm of the average number of collisions which a molecule undergoes before energy transfer occurs, Z_{10}, against the lowest fundamental vibration frequency of the molecule. This falls into two distinct straight lines, one for molecules containing no hydrogen atoms and another for molecules containing two or more hydrogen atoms. Lambert and Salter[24] were unable to provide a satisfactory explanation of this separation of molecules into two groups.

Molecules with no hydrogen atoms have comparatively high moments of inertia, while simple molecules with two or more hydrogen atoms have very low moments of inertia about their principal axes. Table III gives the values of the moments of inertia of some typical molecules as quoted by Herzberg[14].

TABLE III - MOMENTS OF INERTIA

Molecule	$I \times 10^{40}$ (gm.cm.^{2})	Molecule	$I \times 10^{40}$ (gm.cm.^{2})
CH_4	5.33	N_2O	67
CH_3Cl	5.49	CO_2	72
CH_3Br	5.51	Cl_2	115
C_2H_4	5.75	CF_4	221
SiH_4	9.46	CS_2	256
C_2H_2	23.8	CCl_4	735

The rotational velocities of molecules with several hydrogen atoms are much higher than the rotational velocities of molecules with no hydrogen atoms. It therefore seems possible that in molecules with several hydrogen atoms energy is being transferred from the vibrational to the rotational mode. The interaction between the rapidly rotating peripheral atoms of one molecule and the lowest bending vibration of another may be more efficient in transferring energy from vibration than the direct vibrational-translational process. The interconversion of translational and rotational energy occurs more readily than the interconversion of translational and vibrational, or of rotational and vibrational energies, and thus the sequence vibration $\longrightarrow$ rotation $\longrightarrow$ translation is a probable mechanism of vibrational energy transfer in molecules with low moments of inertia. In molecules with high moments of inertia the rotational velocity

may be so low that energy transfer takes place more rapidly through the direct vibration $\longrightarrow$ translation process. The two lines on the Lambert-Salter plot may thus represent two different mechanisms of energy transfer.

Since tetradeuteromethane has a higher moment of inertia and lower peripheral velocity of rotation than methane, vibrational-rotational energy transfer will occur less readily in the deuterated molecule, leading to a longer relaxation time in CD_4 than in CH_4, as observed. Similarly the relaxation time of SiD_4 will be longer than that of SiH_4. In the case of the methyl bromides, the moment of inertia of CD_3Br about the C—Br bond is about twice that of CH_3Br about the same bond. The lowest fundamental (ν_3) of these molecules is the C—Br stretching vibration. It is not now possible to predict the exact nature of the interaction between vibration and rotation, but it is probable that energy is transferred from the stretching vibration to rotation. The more rapidly rotating CH_3Br will thus be more efficient than CD_3Br at vibrational de-excitation, as observed.

In these three pairs of molecules the differences in the moments of inertia are sufficiently great to overcome the opposing effect of lower vibration frequency in the deuterated molecules, and to make the relaxation times of the deuterated molecules longer than those of their hydrogenated counterparts. In the case of the ethylenes $\frac{I_{C_2D_4}}{I_{C_2H_4}} = 1.34$ is much less than $\frac{I_{CD_4}}{I_{CH_4}} = 1.98$, and thus $\frac{\tau_{C_2D_4}}{\tau_{C_2H_4}}$ will be less than $\frac{\tau_{CD_4}}{\tau_{CH_4}}$, and may be less than unity. Experimentally the relaxation time of the deuterated molecule is the shorter, $\frac{\tau_{C_2D_4}}{\tau_{C_2H_4}}$ being 0.54. This, however, is significantly longer

than the maximum value of 0.28 for $\frac{\tau_{C_2D_4}}{\tau_{C_2H_4}}$ predicted for direct vibrational-translational energy transfer, suggesting that vibrational-rotational energy transfer is also occurring in the ethylenes.

Several other cases have been reported in which vibrational-rotational energy transfer may be taking place. Lambert et al.[28] find that the efficiency of $C_2H_4 + SF_6$ collisions is 5.9 times greater than the efficiency of $SF_6 + SF_6$ collisions in deactivating vibrationally excited SF_6. They suggest that the normal vibration-translation process is being facilitated by the relatively low mass and steep intermolecular potential of the C_2H_4 molecule. Now the lowest fundamental of SF_6 is a bond bending vibration, and an alternative explanation may be that energy transfer from this vibration to a rapidly rotating C_2H_4 molecule takes place more rapidly than does direct vibtational-translational energy transfer. $C_2H_4 + SF_6$ collisions would thus be more effective than $SF_6 + SF_6$ collisions in deactivating SF_6, as observed.

The pronounced effect of H_2O on the relaxation time of CO_2 is thought to be due to a quasi-chemical interaction. Van Itterbeek and Mariens[29], and Sette and Hubbard[30] have studied the relative efficiencies of H_2O and D_2O in deactivating vibrationally excited CO_2, and find that the more rapidly rotating H_2O is more efficient than D_2O at several temperatures. It is therefore possible that energy from the bending vibration of CO_2 is being transferred to the rotational mode of water, and that this occurs more readily to H_2O than to D_2O. The same hypothesis can explain Wight's[31] observation that at 19°C H_2O deactivates N_2O 1.7 times more rapidly than does D_2O, and the similar observation of Hudson, McCoubrey and Ubbelohde[27] that H_2O is more efficient than D_2O in deactivating C_2H_4.

Callear[32] has found that the addition of a very small partial pressure of NH_3 or H_2O to NO increases the rate of decay of vibrationally excited NO some 20 times, while Kundsen[33], and Knötzel and Knötzel[34] found that $H_2O + O_2$ and $NH_3 + O_2$ collisions are many thousand times more effective than $O_2 + O_2$ collisions in deactivating vibrationally excited O_2. It is probable that strong, quasi-chemical interactions of the π-complex type are partly responsible for this increased rate of deactivation. But the rotational velocities of the additives to these systems are high, and energy transfer to the rotational mode of H_2O or NH_3 may also be taking place.

McCoubrey, Milward and Ubbelohde[35] have measured the relative catalytic efficiencies of H_2O and D_2O in deactivating vibrationally excited SO_2, and find that D_2O is about 2.7 times as efficient as H_2O. This result apparently contradicts the above hypothesis of vibrational-rotational energy transfer. But it has been established[28] that, if two molecules A and B have vibrational levels of about the same frequency, energy transfer can occur relatively easily between the vibrational modes of the molecules in a "complex collision". If A is a relaxing molecule with a low probability of energy transfer, while B has a much higher transition probability, exchange of vibrational energy followed by rapid deactivation of the vibrational mode of B increases the vibrational-translational probability for A. The ν_1 vibration of SO_2 is 1151 cm.$^{-1}$, while ν_2 of D_2O is 1179 cm.$^{-1}$, a difference of only 28 cm.$^{-1}$. It is probable, therefore, that a vibrational quantum from the 1151 cm.$^{-1}$ mode of SO_2 may be transferred easily to the 1179 cm.$^{-1}$ mode of D_2O. The rate-controlling step in the deactivation of vibrationally excited SO_2 by D_2O will thus be the deactivation of the vibrationally excited D_2O. In the $H_2O + SO_2$ system the most closely matched vibrations are ν_2

of H_2O (1595 cm.$^{-1}$) and ν_3 of SO_2 (1361 cm.$^{-1}$). They are too widely separated for easy vibrational energy exchange, and energy transfer will take place from the vibrational mode of SO_2 to the rotational mode of H_2O, followed by translational-rotational deactivation of H_2O. The rate controlling step in the SO_2 + H_2O system is thus the deactivation of the rotational mode of H_2O. The two systems have two different rate-controlling steps, and it is not possible to predict which will take place more rapidly. In fact it is found that D_2O is the more efficient catalyst, showing that deactivation of vibrationally excited D_2O must take place more rapidly than vibrational-rotational energy transfer from vibrationally excited SO_2 to the rotational mode of H_2O.

The vibrational energy exchange in the SO_2 + D_2O system does not occur in the other two-component systems mentioned above, as the vibrational levels of the components are too widely separated. The qualitative picture of vibrational-rotational energy transfer in molecules with low moments of inertia thus accounts for the longer relaxation times of simple deuterated molecules, explains the two lines on the Lambert-Salter plot, and agrees with the smaller catalytic effect of deuterated molecules in promoting vibrational energy transfer.

CHAPTER 8

QUANTITATIVE DISCUSSION

The above qualitative picture of vibrational-rotational energy transfer is supported by calculations of the relaxation times of the methanes and silanes. We assume that for vibrational-rotational energy transfer, the probability of energy transfer per molecule per second, P_{10}, may be written

$$P_{10} = Z \int_0^\infty p_{10}(v_r) \cdot f(v_r)\ dv_r \qquad \ldots\ldots\ldots (32)$$

where Z is the collision frequency without specification of relative translational velocity, $p_{10}(v_r)$ is the probability of energy transfer between vibration and rotation for a peripheral velocity of rotation v_r, and $f(v_r)$ is the distribution function of rotational velocities.

In the following we use the rigid sphere expression for Z,[36]

$$Z = 4n\sigma^2 \left(\frac{\pi RT}{M}\right)^{1/2} \qquad \ldots\ldots\ldots (33)$$

where n = number of molecules per cm.^{3}

σ = collision diameter

M = molecular weight

and T = absolute temperature.

For a spherical top molecule, the chance of the molecule being in the J^{th} rotational quantum level is

$$p_J = \frac{(2J+1)^2 e^{-E_J/kT}}{Q_r} \qquad \ldots\ldots\ldots (34)$$

where E_J = energy of the J^{th} rotational level = $\dfrac{h^2 J(J+1)}{8\pi^2 I}$

Q_r = rotational partition function = $\dfrac{\sqrt{\pi} \cdot (8\pi^2 IkT)^{3/2}}{sh^3}$

I = principal moment of inertia of the molecule,

and s = symmetry number = 12 for a spherical top.

The classical rotational energy, E_{ROT}, of a spherical top molecule in the J^{th} rotational level is[14]

$$E_{ROT} = \frac{h^2}{8\pi^2 I} \cdot J(J+1) = \frac{1}{2} I \omega^2 \quad \ldots\ldots\ldots (35)$$

where ω = angular velocity of rotation. The classical peripheral velocity of rotation, v_r, in the J^{th} level is thus

$$v_r = \omega r = \frac{hr}{2\pi I} \sqrt{J(J+1)} \quad \ldots\ldots\ldots (36)$$

where r = bond length of the molecule. Eliminating J from eqn. 31 using eqn. 33, we obtain the approximate rotational velocity distribution function:

$$f(v_r) \simeq \frac{16\pi^2 I^2 v_r^2}{h^2 r^2 Q_r} \exp\left(-\frac{I}{2 r^2 kT} \cdot v_r^2\right) \ldots. (37)$$

For a given relative velocity, v_r, the probability of energy transfer in a collision is given by[36]

$$p_{10} = \frac{32\pi^4 m^2 \nu}{h M \alpha^2} \exp\left(-\frac{4\pi^2 \nu}{\alpha v_r}\right) \quad \ldots\ldots (38)$$

for a potential function $V_r = e^{-\alpha r}$, where ν = frequency of the oscillator. The collision in vibrational-rotational energy transfer is essentially a H + H (or D + D) interaction and thus m = reduced mass of a hydrogen (or deuterium) atom for the encounter, and M = reduced mass of the oscillator.

In the molecules of the methanes and silanes, a quantum of vibrational energy is greater than the rotational energy of a molecule in the lower rotational levels. In methane, for example, the quantum of the 1306 cm.$^{-1}$ vibration is 2.6×10^{-13} ergs, while the rotational energy of a methane molecule in the most populous rotational level (the 6th) is only 4.4×10^{-14} ergs. After energy has been transferred from the vibrational to the rotational mode, the relative rotational energy of the colliding molecules is much greater than it was initially. We therefore use the average of the relative rotational energies before and after collision to calculate the transition probability. If E_{ROT} is the relative rotational energy before de-excitation of the excited level, then the relative rotational energy after transfer of energy to the rotational mode of a molecule is $(E_{ROT} + h\nu)$. The relative symmetrised rotational energy, $\overline{E_{ROT}}$ is thus

$$\overline{E_{ROT}} = E_{ROT} + \tfrac{1}{2} h\nu$$

and the relative symmetrised rotational velocity, $\overline{v_r}$, is

$$\overline{v_r} = \left(v_r^2 + \frac{h\nu r^2}{I}\right)^{\frac{1}{2}} \quad \ldots\ldots\ldots\ldots (39)$$

where v_r is the relative rotational velocity before collision. Substitution of this value of $\overline{v_r}$ into eqn. 35 gives

$$p_{10}(v_r) = \frac{32\pi^4 m^2 \nu}{h M \alpha^2} \exp\left[-\frac{4\pi^2 \nu}{\alpha\left(v_r^2 + \frac{h\nu r^2}{I}\right)^{\frac{1}{2}}}\right] \ldots\ldots (40)$$

The expressions for Z (eqn. 33), for $f(v_r)$ (eqn. 37), and for $p_{10}(v_r)$ (eqn. 40) can now be combined in eqn. 32, and numerical integration

of this gives P_{10}. The relaxation time τ for energy transfer via the lowest fundamental vibration is related to P_{10} by the relation

$$\frac{1}{\tau} = P_{10} - P_{01} \simeq P_{10}$$

In the calculation, the values taken for the moments of inertia I and bond lengths r were those given by Herzberg[14]. $\frac{m}{M}$ was taken as unity, and α for the encounter as 3×10^8 cm.$^{-1}$. The value of the collision diameter σ used was 3.4 Å for the methanes and 4 Å for the silanes. Eqn. 32 then reduced to a form suitable for numerical integration. At 298°K, for example, the equation was

$$P_{10} = 1.007 \times 10^{-1} \int_0^\infty v_r^2 \exp\left[-5.438 \times 10^{-11} \times v_r^2 - \frac{5.153 \times 10^6}{\sqrt{v_r^2 + 5.792 \times 10^{10}}} \right] dv_r$$

for CH_4, while for CD_4 it was

$$P_{10} = 3.800 \times 10^{-1} \int_0^\infty v_r^2 \exp\left[-1.071 \times 10^{-10} \times v_r^2 - \frac{3.928 \times 10^6}{\sqrt{v_r^2 + 2.242 \times 10^{10}}} \right] dv_r$$

P_{10} was calculated for the methanes and silanes with and without symmetrisation of the rotational energy. The resulting relaxation times are summarised in Table IV.

TABLE IV - CALCULATED RELAXATION TIMES (in seconds)

	WITHOUT SYMMETRISATION			WITH SYMMETRISATION		
	298°K	348°K	τ_{298}/τ_{348}	298°K	348°K	τ_{298}/τ_{348}
CH_4	1.0×10^{-6}	3.2×10^{-7}	3.1	5.6×10^{-8}	2.6×10^{-8}	2.1
CD_4	1.85×10^{-6}	6.0×10^{-7}	3.1	1.8×10^{-7}	8.6×10^{-8}	1.9
$\frac{\tau_{CD_4}}{\tau_{CH_4}}$	1.85	1.88		3.2	3.3	
SiH_4	1.5×10^{-8}	7.0×10^{-9}	2.1	2.1×10^{-9}	1.2×10^{-9}	1.75
SiD_4	1.9×10^{-8}	8.3×10^{-9}	2.3	3.3×10^{-9}	2.3×10^{-9}	1.45
$\frac{\tau_{SiD_4}}{\tau_{SiH_4}}$	1.28	1.19		1.57	1.87	

Table V gives the experimental results for comparison.

TABLE V - EXPERIMENTAL RELAXATION TIMES (in seconds)

	298°K	348°K	τ_{298}/τ_{348}
CH_4	2.03×10^{-6}	1.10×10^{-6}	1.85
CD_4	3.90×10^{-6}	2.50×10^{-6}	1.56
$\frac{\tau_{CD_4}}{\tau_{CH_4}}$	1.92	2.27	
SiH_4	1.15×10^{-7}	1.04×10^{-7}	1.11
SiD_4	1.96×10^{-7}	1.78×10^{-7}	1.10
$\frac{\tau_{SiD_4}}{\tau_{SiH_4}}$	1.70	1.71	

Although the relaxation times calculated without symmetrisation show reasonable agreement with the experimental values, the calculated temperature dependence is too steep. Symmetrisation reduces this steepness, but the absolute values of the relaxation times are consistently in error by a factor of 50 (probability too high). Such inaccuracies are not surprising in view of the drastic approximations made in the calculation. The important result is, however, that the calculated effect of isotopic substitution is in line with experiment. The conventional translational-vibrational treatment predicts the opposite effect of isotopic substitution to that observed, and this strongly suggests that the mechanism of vibrational deactivation to rotation is correct.

REFERENCES

1. Roberts, "Heat and Thermodynamics", Blackie, London, 1954.
2. Pierce, Proc. Amer. Acad., 60, 271 (1925).
3. Pielemier, Phys. Rev., 34, 1184 (1929).
4. Scott, Cook, Brickwedde, Bur. Stand. J. Res., 7, 935 (1931).
5. Alleman, Phys. Rev., 55, 87 (1939).
6. Krasnooshkin, Phys. Rev., 65, 190 (1944).
7. Stewart and Stewart, J. acoust. Soc. Am., 24, 22 (1952).
8. Blythe, Ph.D. thesis, Edinburgh, 1962.
9. Clusius and Riccoboni, Z. phys. chem., B, 38, 81 (1938).
10. Johnston and Davies, J.A.C.S., 56, 271 (1934).
11. Johnston and Walker, J.A.C.S., 55, 172 (1933).
12. Tilton, Bur. Stand. J. Res., 13, 111 (1934).
13. Holborn and Otto, Z. Phys., 33, 1, (1925).
14. Herzberg, "Molecular Spectra and Molecular Structure", Part II, Van Nostrand, New York, 1945.
15. Hirschfelder, Bird and Spotz, Trans. Amer. Soc. Mech. Eng., 71, 291 (1949).
16. Tindal, Straley and Nielsen, Phys. Rev., 62, 151 (1942).
17. McKean, personal communication, 1961.
18. Stock and Somieski, Ber., 49, 111 (1916).
19. Meal and Wilson, J. chem. Phys., 24, 385 (1956).
20. Griffith, J. appl. Phys., 21, 1319 (1950).
21. Edmonds and Lamb, Proc. Phys. Soc., A, 72, 940 (1958).
22. Cottrell and Martin, Trans. Faraday Soc., 53, 1157 (1957).
23. Eucken and Aybar, Z. phys. Chem., B, 46, 195 (1940).
24. Lambert and Salter, Proc. Roy. Soc., A, 253, 277 (1959)
25. Corran, Lambert, Salter and Warburton, Proc. Roy. Soc., A, 244, 212 (1958).

26. Amme and Legvold, J. chem. Phys., 30, 163 (1959).

27. Hudson, McCoubrey and Ubbelohde, Proc. Roy. Soc., A, 264, 289 (1961).

28. Lambert, Edwards, Pemberton and Stretton, Disc. Faraday Soc., 33 (1962), in the press.

29. Van Itterbeek and Mariens, Physica, 7, 125 (1940).

30. Sette and Hubbard, J. acoust. Soc. Amer., 25, 994 (1953).

31. Wight, J. acoust. Soc. Amer., 28, 459 (1956).

32. Callear, Disc. Faraday Soc., 33 (1962), in the press.

33. Kundsen, J. acoust. Soc. Amer., 6, 199 (1935).

34. Knötzel and Knötzel, Ann. Physik, 2, 393 (1948).

35. McCoubrey, Milward and Ubbelohde, Proc. Roy. Soc., A, 264, 299 (1961).

36. Cottrell and McCoubrey, "Molecular Energy Transfer in Gases", Butterworths, London, 1961.

ACKNOWLEDGEMENTS

It has been a very stimulating experience to work with Professor Cottrell, and I wish to thank him for suggesting this research problem and for his helpful advice at all times. I have also had many useful discussions with Mr. A.R. Blythe and Mr. A.W. Read, and I am grateful to Mr. W.B. Brown who first suggested that rotation might be important in intermolecular energy transfer.

I wish to thank: D.S.I.R. for providing a maintenance grant for three years; Dr. J.L. Duncan for the infra-red analyses; and Miss E.L. Metcalfe, Mr. J.A.G. Dominguez, and Dr. C.H.J. Wells for the gas chromatographic analyses. I also wish to thank the University of Edinburgh for providing facilities for this research.